Evaluation of 3-hydroxy fatty acids as a pH and temperature proxy in soils from temperate and tropical altitudinal gradients

Arnaud Huguet, Sarah Coffinet, Anthony Roussel, Félix Gayraud, Christelle Anquetil, Laurent Bergonzini, Giuliano Bonanomi, David Williamson, Amos Majule, Sylvie Derenne

Evaluation of 3-hydroxy fatty acids as a pH and temperature proxy in soils from temperate and tropical altitudinal gradients

Arnaud Huguet [a*], Sarah Coffinet [a, b], Anthony Roussel [a], Félix Gayraud [a], Christelle Anquetil [a], Laurent Bergonzini [c], Giuliano Bonanomi [d], David Williamson [e], Amos Majule [f], Sylvie Derenne [a]

[a] *Sorbonne Université, CNRS, EPHE, PSL, UMR METIS, F-75005 Paris, France*
[b] *MARUM – Center for Marine Environmental Sciences, University of Bremen, 28359 Bremen, Germany*
[c] *Université Paris Saclay, UPS Univ Paris 11, CNRS, GEOPS, F-91405 Orsay cedex, France*
[d] *Dipartimento di Agraria, University of Naples Federico II, via Università, 100 Naples, Italy*
[e] *Sorbonne Université, IRD, MNHN, CNRS, UMR LOCEAN, Centre IRD France Nord, F-93143 Bondy cedex, France*
[e] *Institute of Resource Assessment, University of Dar Es Salaam, P.O. Box 35097, Dar Es Salaam, Tanzania*

ABSTRACT

3-OH FAs containing 10 to 18 C and a hydroxyl group in third position are characteristic components of Gram-negative bacteria. These compounds were previously used to detect and quantify Gram-negative bacterial communities in various types of samples, from terrestrial, aquatic and atmospheric environments. The relative abundance of 3-OH FAs in soils was recently shown to vary with mean annual air temperature (MAAT) and pH in soils from Mt. Shennongjia (China). In the current study, the concentrations and abundances of 3-OH FAs were determined in soils from altitudinal transects under tropical and temperate climates – Mt. Rungwe (SW Tanzania) and Mt. Majella (Central Italy), respectively. The aim was to (i) examine and compare the distributions of 3-OH FAs in soils from different climatic zones and to (ii) investigate the potential of 3-OH FAs as temperature and pH proxies. When combined with previously published data, a moderate correlation (R^2 0.62) between the summed *iso* and *anteiso* to the total amount of normal 3-OH FAs (RIAN index) and pH is obtained. We show

* Corresponding author. Tel: + 33-144-275-172; fax: +33-144-275-150.
E-mail address: arnaud.huguet@sorbonne-universite.fr (A. Huguet).

that Gram-negative bacteria respond in the same way to temperature variations in soils from different latitudes, with a relative increase of the *anteiso* to normal 3-OH FA ratios of the C_{15} and C_{17} compounds (RAN_{15} and RAN_{17} indices, respectively) with decreasing temperature. Nevertheless, the intercepts of the relationships between RAN_{15} and MAAT are mountain-dependent, suggesting that regional calibrations may be required to use RAN_{15} as a temperature proxy. In contrast with RAN_{15}, the statistical similarity of the local relationships between RAN_{17} and MAAT leads to a combined calibration (R^2 0.60, residual mean error 5.1 °C) covering a wide range of temperature (ca. 0 – 25 °C). As 3-OH FAs seem well-preserved in sedimentary archives, this strengthens the potential of these compounds as a temperature and pH proxy for paleoreconstructions in terrestrial settings.

Keywords: 3-Hydroxy fatty acids; soils; altitudinal transects; environmental proxies

1. Introduction

Investigating past climatic variations is essential to understand and predict future environmental changes. Paleoclimate studies are chiefly carried out for marine environments because environmental proxies were mainly developed and used for oceanic settings. The composition and mechanism of formation of marine sediments are indeed less complex than the highly heterogeneous continental settings. Several environmental proxies based on organic (e.g. the alkenone unsaturation index – $U^{k'}_{37}$; Brassell et al., 1986; the tetraether index of 86 carbon atoms – TEX_{86}; Schouten et al., 2002) and inorganic (e.g. Mg/Ca ratio and $^{18}O/^{16}O$ ratio of foraminifera; Erez and Luz, 1983; Elderfield and Ganssen, 2000) fossil remains were notably developed for the reconstruction of sea surface temperatures. However, it is essential to develop new proxies also applicable in continental environments to assess climatic variability over the continents and improve the understanding of past global climate.

Membrane lipids produced by some microorganisms can be used to this aim. Environmental stresses can alter membrane fluidity and permeability, thus affecting the proper functioning of the cell. Microorganisms (bacteria, archaea and some eukaryotes) are able to adjust their membrane composition in response to the prevailing environmental conditions in order to maintain an appropriate fluidity and ensure the optimal state of the cellular membrane (e.g. Hazell and Williams, 1990; Denich et al., 2003), so-called "homeoviscous adaptation" (Sinensky, 1974). Bacteria can thus change the number of unsaturations, ramifications or chain length of their membrane lipids – mainly fatty acids – in response to varying environmental conditions (e.g. Prado et al., 1988; Suutari and Laakso, 1992). In the same way, the structure of glycerol dialkyl glycerol tetraethers (GDGTs), which are membrane lipids biosynthesised by archaea and some bacteria, is known to be related to environmental parameters (Schouten et al., 2013 and references therein). Bacterially-derived branched glycerol dialkyl glycerol tetraethers (brGDGTs) have especially been the object of growing interest, as they are, to date, the only available organic proxies which can be used for terrestrial temperature and pH reconstructions (e.g. Peterse et al., 2014; Zheng et al., 2015). Nevertheless, paleoenvironmental data derived from brGDGTs have to be interpreted with care, as their source microorganisms remain unknown, although some might belong to the phylum *Acidobacteria* (Sinninghe Damsté et al., 2011, 2014, 2018). Each environmental proxy has its strengths and limitations, related to several factors (biological, environmental, physical etc.). The development of new environmental proxies, independent of and complementary to those derived from brGDGTs, is required to improve the reliability and accuracy of terrestrial environmental reconstructions and to provide constraints on brGDGT applications.

Recently, Wang et al. (2016) suggested that other bacterial lipids, so called 3-hydroxy fatty acids (3-OH FAs), could be used as such a proxy. These compounds, containing 10 to 18 C

and a hydroxyl group in third position, are characteristic components of the Gram-negative bacterial lipopolysaccharide (LPS). The LPS is a major constituent of the external surface layer of these microorganisms. It is composed of three parts: (i) a polysaccharide chain (O antigen); (ii) a core oligosaccharide and (iii) the lipid A, the most internal region of the LPS, mainly constituted of 3-OH FAs (Raetz et al., 2007). Gram-negative bacteria are ubiquitous in terrestrial and aquatic environments. 3-OH FAs were previously used to detect and quantify Gram-negative bacterial communities in various types of samples, such as marine dissolved organic matter (Wakeham et al., 2003), atmospheric aerosols (Cheng et al., 2012), fresh snow (Tyagi et al., 2015) or soils (Zelles et al, 1995). Nevertheless, only little information is available regarding the effect of environmental parameter variations on the 3-OH FA structures. Recently, 3-OH FAs were analysed in 26 soils located between 315 and 2840 m elevation along Mt. Shennongjia (China; Wang et al., 2016). Significant correlations were obtained between the relative abundance of these compounds and temperature or pH. The ratio of the summed *iso* and *anteiso* to the total amount of *normal* 3-OH FAs (defined as the RIAN index) correlated with soil pH, and the *anteiso* to *normal* 3-OH FA ratio for the C_{15} and C_{17} compounds (RAN_{15} and RAN_{17} indices, respectively) correlated with MAAT (Wang et al., 2016). The RAN_{15} and RIAN were very recently used to reconstruct Holocene temperature and hydrological changes from a stalagmite collected in Central China (Wang et al., 2018). This suggests that 3-OH FA-based proxies are promising tools for paleoenvironmental reconstructions. Nevertheless, to date, the applicability of 3-OH FAs as temperature and pH proxies has only been investigated in Central China so should be tested in other regions of the world.

In the present study, concentrations and abundances of 3-OH FAs were determined in soils from two contrasting altitudinal transects: one under tropical climate – Mt. Rungwe, SW Tanzania, and the other one under temperate climate – Mt. Majella, Central Italy. The aims

were (i) to examine and compare the distributions of 3-OH FAs in soils from different climatic zones, including the Chinese samples previously analysed by Wang et al. (2016) and (ii) to investigate the potential of 3-OH FAs as temperature and pH proxies.

2. Material and methods

2.1. Sites and sampling

Soil samples were collected along two different altitudinal gradients. The first site is Mt. Rungwe (2960 m) located in the southwest of Tanzania, described in detail by *e.g.* Williamson et al. (2014) and Coffinet et al. (2017). Briefly, it experiences a tropical climate, with an alternating hot humid season (November to May) and a cold dry season (June to October), the precipitation reaching 2400 mm/yr on average with similar amounts from the base to the top of the mountain (Bergonzini, 1998). Natural vegetation along the altitudinal transect includes Zambezian Miombo-type woodland at low altitude and Afromontane vegetation at higher altitude. Various soil types derived from geological bedrock materials (volcanic ash and pumice) are encountered along Mt. Rungwe, eutric Leptosols, umbric Nitisols and haplic Lixisols being predominant (Tilumanywa, 2013). Soils in the high grasslands are thin and quite rocky, while those on the steep slopes of Mt. Rungwe are predominantly dark greyish and dark brown with sandy and clay loams, and those of the main arable lands are coarse or medium-textured, ranging from sandy loams to alluvial (Tilumanywa, 2013). MAAT measurements with temperature loggers during 1 yr (Davis Instruments, Hayward, CA, USA) at three altitudinal points showed a decrease from 25.6 °C at 540 m to 22.6 °C at 920 m and 16.9 °C at 1720 m. MAAT at other altitudes were linearly extrapolated from these recorded temperature data (Table 1). 3-OH FAs were analysed in 21 surface soils (A horizon; 0-5 cm depth) collected between ca. 500 and 2800 m along Mt. Rungwe in April and December 2012 and November 2016. Samples were kept at room

138 temperature for a limited amount of time (ca. 2 weeks) before being sent to France by
139 airplane.

140 The second site is Mt. Majella (2794 m elevation) located in Abruzzo, Central Italy and
141 was described in detail by *e.g.* Bemigisha et al. (2009) and Bonanomi et al. (2016). Climate is
142 Mediterranean at the lower part of the gradient and changes to subalpine-alpine humid type at
143 the upper part. Along the southern side of the massif, where samples were collected, mean
144 annual precipitation (MAP) changes (Table 1 and Supp. Table 1), ranging between ca. 800-
145 900 mm/year at the lower part of the gradient (0-1000 m a.s.l.) and ca. 1200-1300 mm/year at
146 the upper part (> 2000 m a.s.l.). A sharp vertical zonation of vegetation type is observed,
147 including olive orchards at the bottom (ca. 300 m a.s.l.), forest and low elevation grasslands in
148 between (800 – 1850 m a.s.l) and high altitudinal grasslands above (Bonanomi et al., 2016).
149 MAAT decreases from 14.6 °C at 300 m to 3.1 °C at 2405 m and 0.03 °C at 2730 m (Stanisci
150 et al., 2005). Soil is spatially variable from shallow rendzic Leptosol with xeromoder humus
151 and basic pH to skeletic Leptosol, the latter covered with flat frost-shattered gravel stones on
152 the plateau and bare solifluxed steep slopes (Bonanomi et al., 2016). 11 surficial soil samples
153 (0-5 cm depth) were collected between 400 and 2800 m along Mt. Majella in December 2016
154 and were immediately frozen at -20 °C after sampling. Samples from Mt. Rungwe and Mt.
155 Majella were stored at -20 °C and then freeze-dried, ground and homogenized.

156

157 *2.2. pH and elemental analysis*
158

159 The pH of freeze-dried samples was measured in ultrapure water (Milli-Q, Millipore with a
160 1:2.5 soil water ratio (Table 1). The decarbonation of soil samples from Mt. Rungwe collected
161 in 2012 and the subsequent organic carbon content (C_{org}) elemental analysis was performed at
162 the Service Central d'Analyse du CNRS for soil samples, as reported in Coffinet et al. (2014).
163 All the other samples (Mt. Rungwe and Mt. Majella soils collected in 2016) were

decarbonated with HCl and neutralized with deionized water (cf. Huguet et al., 2013a). C_{org} content was then determined using an Elementar Vario Pyrocube.

2.3. Sample preparation

Preparation of samples for 3-OH FA analysis followed the procedure of Wang et al. (2016) with slight modifications. Briefly, ca. 10 g of freeze-dried and ground soil were subjected to acid hydrolysis. Whereas only free 3-OH FAs are obtained upon direct solvent extraction, additional compounds bound to LPS of Gram-negative bacteria can be released through the hydrolysis step (Wang et al., 2012, 2016). Acid hydrolysis was shown to be more efficient in extracting 3-OH FAs from soil samples than saponification, suggesting that most of these molecules are linked to macromolecules by amide bonds in soils, the latter being difficult to cleave off by saponification (Yang et al., 2016). Consequently, soil samples were subjected to acid digestion rather than saponification in this study. They were refluxed with 3M HCl aq. for 3 h using a silicon oil bath heated at 130 °C. After cooling, the suspension was centrifuged for 10 min at 15 °C and 3500 rpm and the supernatant transferred to a separation funnel. The residue was then sequentially extracted with a mixture of dichloromethane (DCM):MeOH (1:1, v/v; 2×) and DCM (2×). Each extraction was followed by centrifugation and combination of all extracts in the separation funnel. The DCM phase was separated from the MeOH/H_2O layer, which was again extracted with DCM (3×). The DCM fractions were combined and rotary-evaporated. The lipid extract obtained after acid hydrolysis of the soil was methylated with HCl-MeOH 1 M at 80 °C for 1 h and then separated into 3 fractions over a silica column (activated at 150 °C overnight) using (i) 30 mL of heptane/EtOAc (98:2), (ii) 30 mL of EtOAc and (iii) 30 mL of MeOH. OH-FA methyl esters (FAMEs) eluted only in the second fraction. The OH-FAMEs, diluted in DCM, were derivatised with a solution of *N*,*O*-bis(trimethylsilyl)trifluoroacetamide (BSTFA) – Trimethylchlorosilane (TMCS) 99:1 (Grace

190 Davison Discovery Science, USA) at 70 °C for 20 min before gas chromatography-mass
191 spectrometry (GC-MS) analysis.
192
193 *2.4. 3-OH FA analysis*
194
195 3-OH FAs were analysed using an Agilent Network 6890 GC System coupled with a 5973
196 Mass Selective Detector, with electron impact at 70 eV. A Restek RXI-5 Sil MS silica column
197 (30 m × 0.25 mm i.d., 0.50 µm film thickness) was used with He as the carrier gas at 1
198 ml/min. The GC oven program was: 70 °C to 200 °C at 10 °C/min, then to 310 °C (held 45
199 min) at 3°C/min. Samples were injected in splitless mode and the injector was at 280 °C.
200 Quantification of 3-OH FAs was performed by comparing the integrated signal from the
201 respective compound with that from an analogous deuterated internal standard (3-
202 hydroxytetradecanoic acid, 2,2,3,4,4-d5; Sigma-Aldrich, France).
203 A 1:1 mixture of the internal standard and non-deuterated C_{12}, C_{14} and C_{18} 3-OH FA
204 standards (Larodan Chemicals, Sweden) was injected to determine the response factor of the
205 internal standard relative to 3-OH FAs before soil sample analyses. The standard mixture was
206 methylated and silylated as described above before injection. Non-deuterated TMSi methyl
207 ester derivatives of 3-OH FAs showed an intense diagnostic fragment ion (*m/z* 175) as
208 observed by e.g. Wang et al. (2016), whereas that of the deuterated internal standard is *m/z*
209 178. GC-MS analysis of the mixture resulted in an equivalent response factor for the
210 deuterated standard relative to the non-deuterated 3-OH FA compounds, whatever their chain
211 lengths.
212 In soil samples from Mt. Rungwe and Mt. Majella, the TMSi methyl ester derivatives of 3-
213 OH FAs were identified from their retention times and mass spectra. In addition to m/z 175,
214 other characteristic ions include $M^+ - 15$ (base peak), $M^+ - 31$, and *m/z* 89, 103, 133 and 159
215 (e.g. Volkman et al., 1999; Wang et al., 2016). A solution of the deuterated 3-OH FA internal

standard, methylated as described above (cf. section 2.3.), was added to each sample after acid hydrolysis, solvent extraction and separation on silica column. Typically, 1.5 µg of methylated internal standard was added to 5 mg of the EtOAc fraction from the extract. This mixture was then silylated with BSTFA-TMCS, as previously described, and then analysed by GC-MS. The coefficient of variation (CV) for triplicate injections of 5 samples was 0.7% for 3-OH FAs.

The RIAN index was calculated as follows (Wang et al., 2016):

$$RIAN = -\log [(I+A)/N] \quad (1)$$

where *I*, *A* and *N* represent the sum of all the *iso*, *anteiso* and *normal* 3-OH FAs respectively. In the same way, the RAN_{15} and RAN_{17} indices were defined as follow (Wang et al., 2016)

$$RAN_{15} = [anteiso\text{-}C_{15}] / [normal\text{-}C_{15}] \quad (2)$$

$$RAN_{17} = [anteiso\text{-}C_{17}] / [normal\text{-}C_{17}] \quad (3)$$

and correspond to the ratios of *anteiso* to *normal* C_{15} and C_{17} 3-OH FAs, respectively. The analytical error based on triplicate injections was 0.006 for RIAN, 0.18 for RAN_{15} and 0.05 for RAN_{17}.

2.5. BrGDGT analysis

BrGDGT data have been previously published for (i) 19 of the 26 soil samples from Mt. Shennongjia (Yang et al., 2015) and for (ii) 16 of the 21 soil samples from Mt. Rungwe collected in 2012 (Coffinet et al., 2014). BrGDGT analysis of the aforementioned samples was performed using the traditional method based on a normal phase separation with a cyano column, which does not allow the separation of 5- and 6-methyl isomers.

Regarding soils from Mt. Majella, sample preparation was similar to that detailed by Coffinet et al. (2014). In these samples, brGDGTs were analysed with a Shimadzu LCMS-

2020 in selected ion monitoring mode using a procedure modified from Yang et al. (2015) and Hopmans et al. (2016) allowing the separation of 5- and 6-methyl isomers. Separation was achieved with two silica columns in tandem (150 mm × 2.1 mm, 1.9 µm, Thermo Finnigan; USA) thermostated at 40 °C. Injection volume was 10 µl. GDGTs were first eluted isocratically with 82% A/18% B for 25 min (A = hexane, B = hexane/isopropanol 9/1, v/v). The following linear gradient was subsequently used: 82% A/18% B to 65% A/35% B in 25 min, followed by 65% A/35 % B to 100% B, maintained for 10 min and then back to 82% A/18% B in 10 min, maintained for 30 min. The flow rate was set at 0.2 ml/min. Semi-quantification of brGDGTs was performed by comparing the integrated signal of the respective compound with the signal of a C_{46} synthesized internal standard (Huguet et al., 2006) assuming their response factors to be identical.

The MBT and CBT indices were calculated as follows (Weijers et al., 2007):

$$MBT = \frac{[Ia+Ib+Ic]}{[Ia+Ib+Ic]+[IIa+\ IIb+IIc]+[IIIa+IIIb+IIIc]+[II'a+II'b+II'c]+[III'a+III'b+III'c]} \quad (4)$$

$$CBT = -\log\left(\frac{[Ib]+[IIb+II'b]}{[Ia]+[IIa+II'a]}\right) \quad (5)$$

The Roman numerals correspond to the structures presented in De Jonge et al. (2014). The 6-methyl brGDGTs are denoted by an accent after the roman numerals for their corresponding 5-methyl isomers.

MBT' was calculated according to Peterse et al. (2012):

$$MBT = \frac{[Ia+Ib+Ic]}{[Ia+Ib+Ic]+[IIa+\ IIb+IIc]+[IIIa]+[II'a+II'b+II'c]+[III'a]} \quad (6)$$

MBT'$_{5Me}$ was calculated using the equation of De Jonge et al. (2014):

$$MBT'_{5Me} = \frac{[Ia+Ib+Ic]}{[Ia+Ib+Ic]+[IIa+IIb+IIc]+[IIIa]} \quad (7)$$

For soils from Mt. Shennongjia, MAAT was previously estimated by Wang et al. (2016) using a local calibration (Yang et al., 2015):

$$MAAT = 2.06 + 28.13 \times MBT – 9.06 \times CBT \quad (8)$$

Along Mt. Rungwe, MAAT was estimated using the East African regional calibration proposed by Coffinet et al. (2017):

$$MAAT = – 8.76 \times CBT + 24.24 \times MBT' + 9.60 \quad (8)$$

Regarding Mt. Majella, MAAT was reconstructed using the global soil calibration by De Jonge et al. (2014) as no local or regional calibration exists for this mountain:

$$MAAT = – 8.57 + 31.45 \times MBT'_{5Me} \quad (9)$$

The 6-methyl brGDGTs are excluded from the calibration by De Jonge et al. (2014), improving the accuracy of MAT reconstructions compared to previous global soil calibrations including both 5- and 6-methyl brGDGTs (Weijers et al., 2007; Peterse et al., 2012).

2.6. Statistical analyses

All statistical analyses were performed using the software Graph Pad Prism 7.04 (Graph Pad Software Inc.). Relationships of 3-OH FA distribution with MAAT and soil pH in specific altitudinal transects as well as in the complete dataset were evaluated based on the Pearson coefficient of determination r^2 and were considered as significant when the *p*-value of the correlation coefficient was lower than 0.05. Whatever the correlation, samples with standardized residuals higher than 2 or lower than -2 were identified as outliers. Comparison of the regressions obtained from the different mountains was performed using homogeneity of slope test followed by an analysis of co-variance in order to compare the slopes and intercepts

of the correlations, respectively. Differences between soil datasets were considered significant when *p*-value was lower than 0.05.

3. Results and discussion

3.1. Distribution and concentration of 3-OH FAs

3-OH FAs were detected in all soil samples from Mt. Majella and Mt. Rungwe (Supp. Table 1), as shown for example in the chromatogram of a sample collected at 520 m altitude along Mt. Rungwe (Fig. 1). The carbon number of the 3-OH FAs in soils from these two mountains varied between C_{10} and C_{18}, with even and *normal* chain compounds dominant over even, *iso* and *anteiso* homologs (Fig. 1; Supp. Table 2), as observed for soils from Mt. Shennongjia (Wang et al., 2016). It should be noted that 3-OH FAs with 19 to 26 carbon atoms were also detected in soils from Mt. Rungwe and Mt. Majella and represented < 10 % of total 3-OH FAs (i.e. C_{10} to C_{26} homologs; data not shown). These long chain 3-OH FAs were previously shown to be widely distributed in microorganisms, being produced by *e.g.* yeasts, fungi, and Gram-positive bacteria in addition to Gram-negative ones (Zelles,1997; Kock et al., 1999). In this paper, only 3-OH FAs with 10 to 18 C, typical for Gram-negative bacteria (Wilkinson et al., 1988), will be considered.

About 60 to 90 % of total 3-OH FAs (with a chain length of 10 to 18 C) were of even carbon number (Supp. Table 2), as typically observed in the LPS of Gram-negative bacteria (Wilkinson, 1988). *n*-C_{14}, C_{16} and C_{18} were the most abundant 3-OH FAs in soils from both Mt. Rungwe and Mt. Majella (*ca.* 50 to 60 % and 40 to 50 % of total 3-OH FAs for Mt. Rungwe and Mt. Majella, respectively; Supplementary Table 2). Odd 3-OH FAs were dominated by C_{15} and C_{17} homologs, with *iso* compounds being *ca.* 2 to 10 times more abundant than those with *anteiso* and normal chains (Supplementary Table 2). Odd short-chain homologs (C_{11} and C_{13}) were generally present at low concentration in soil samples (each representing less than 5% of total 3-OH FAs), and some of them were even not detected

311 in some soils (e.g. *anteiso* C_{11} and *n*-C_{11} along Mt. Majella; Supp. Table 2). The different 3-
312 OH FAs reported in this study were similarly observed in a wide range of environmental
313 samples, *e.g.* atmospheric dust (Saraf et al., 1997; Tyagi et al., 2015), marine dissolved
314 organic matter (Wakeham et al., 2003), stalagmites (Wang et al., 2012, 2018), sediments
315 (Mendoza et al., 1986; Wakeham, 1999) as well as in biomass from Gram-negative bacterial
316 strains (e.g. Pinkart and White, 1998). The dominant homologs were shown to differ from
317 sample to sample in all environmental settings, including soils from Mt. Majella and Mt.
318 Rungwe (Supp. Table 2). This likely reflects variations in distribution of 3-OH FAs in the
319 LPS of the Gram-negative bacterial species (e.g. *Pseudomonas* species, Pinkart and White,
320 1998; *Geobacter* species, Hedrick et al., 2009). Thus, 3-OH FAs with either 10, 12 or 14 C
321 were shown to be predominant among the different *Pseudomonas* species (Oyaizu and
322 Komagata, 1982), while the most abundant homologs of the genera Bacteroides and
323 Fusobacterium were either C_{14} or C_{16} 3-OH FAs (Miyagawa et al., 1979).
324 Concentrations of Gram-negative bacterial 3-OH FAs with respect to dry soil weight are
325 similar for soils from Mt. Rungwe (1.1 to 24.2 µg/g soil; mean 7.8 µg/g soil) and Mt. Majella
326 (0.8 to 21.3 µg/g soil, mean 10.2 µg/g soil; Supp. Table 1) and are in the same range as those
327 previously observed in one surficial Finnish soil (16.8 µg/g soil; Keinänen et al., 2003) and
328 soils from various locations under different cultivation types (0.4 to 6.3 µg/g ; Zelles, 1999
329 and references therein). Nevertheless, when normalised to total organic carbon, 3-OH FA
330 concentrations were significantly higher ($p < 0.05$) in soils from Mt. Rungwe (17.9 to 1062.5
331 µg/g C_{org}; mean 197.41 µg/g C_{org}) than in those from Mt. Majella (2.1 to 103.9 µg/g C_{org};
332 mean 43.2 µg/g C_{org}; Table 1), due the higher C_{org} contents in Mt. Majella (29 ± 9.0 %) than in
333 Mt. Rungwe samples (5.0 ± 3.0 %; Table 1). Several environmental parameters, such as
334 vegetation cover or annual amount of precipitation, which differ significantly between Mt.
335 Majella and Mt. Rungwe (cf. section 2.1.), might impact the growth of Gram-negative

bacteria and thus the production of 3-OH FAs in soils. The higher concentrations of Gram-negative bacterial 3-OH FA concentrations along Mt. Rungwe than along Mt. Majella might at least be partly due to both quantitative and qualitative differences in soil organic matter (SOM) composition between the two mountains. The abundance and composition of bacterial communities in soils were indeed reported to be directly influenced by the amount and quality of soil organic carbon, the proportions of Gram-negative bacteria generally increasing in soil in the presence of fresh and labile organic substrates (e.g. Nemergut et al., 2010; Fanin et al., 2014). In any case, the variability of 3-OH FA concentrations along each mountain is independent of elevation, as 3-OH FA concentrations do not correlate with elevation neither along Mt. Rungwe (R^2 0.11) nor along Mt. Majella (R^2 0.09).

3.2. 3-OH FA-derived proxies

The correlations between the relative abundance of the 3-OH FAs in soils from Mt. Rungwe and Majella and environmental parameters were investigated using the different indices recently defined by Wang et al. (2016) – RIAN, RAN_{15} and RAN_{17}.

3.2.1. RIAN index

The ratio of the sum of *iso* and *anteiso* 3-OH FAs from Gram-negative bacteria to the total amount of *normal* 3-OH FAs in the C_{12}-C_{18} range, defined as the RIAN index (Eq. 10) was previously shown to correlate negatively with soil pH along Mt. Shennongjia (Wang et al., 2016):

$$RIAN = 1.11 - 0.10 \times pH \ (n = 26;\ R^2\ 0.70;\ p < 0.001) \quad (10)$$

This index was calculated for all soil samples from Mt. Rungwe and Mt. Majella. RIAN ranged between 0.31 and 0.80 along Mt. Rungwe and between 0.16 and 0.43 along Mt. Majella (Table 1). In contrast with Mt. Shennongjia, RIAN does not correlate with measured

362 pH neither along Mt. Rungwe (R^2 0.10) nor along Mt. Majella (R^2 0.16; Fig. 2a). The absence
363 of local correlation between RIAN and pH along Mt. Majella and Mt. Rungwe may be due to
364 the fact that pH varies in a much smaller range (ca. 1.5 units; Table 1) in soils from these two
365 mountains than in those from Mt. Shennongjia (ca 3.5 units; Wang et al., 2016). A similar
366 hypothesis may be put forward to explain (i) the moderate / very poor correlations between
367 brGDGT-based CBT and pH along Mts. Rungwe (R^2 0.31, p = 0.025; data not shown) and
368 Majella (R^2 0.03, p = 0.70; cf. Supp. Table 3 for CBT values), respectively and (ii) the
369 contrast with Mt. Shennongjia, where CBT was significantly correlated with pH (R^2 0.74,
370 $p<0.001$; Yang et al., 2015). As CBT and RIAN are poorly correlated with soil pH along Mts.
371 Rungwe and Majella, no significant correlation between RIAN and CBT can be observed
372 along these two mountains, in contrast with Mt. Shennongjia (Fig. 2b).
373 So as to overcome the limitation associated with the restricted pH range in a given
374 mountain, RIAN data from the three mountains were combined. In the resulting extended
375 dataset, with 65 samples covering a large range of pH (4.5 to 8.7), each soil was considered as
376 an independent and individual sample. This combination of data resulted in a significant
377 negative correlation between RIAN and pH (Fig. 2a):
378 $$RIAN = 1.16 - 0.12 \times pH \quad (11)$$
379 Eq. 11 presents similar slope and intercept as the initial relationship between RIAN and pH
380 observed along Mt. Shennongjia (Eq. 10; Wang et al., 2016).
381 Reconstruction of pH using RIAN can be performed using Eq. 12:
382 $$pH = 8.63 - 5.36 \times RIAN \ (n = 63;\ R^2\ 0.62;\ RMSE\ 0.56;\ n_{outliers} = 2;\ p < 0.001) \quad (12)$$
383 Two outliers (one from Mt. Rungwe and one from Mt. Majella; Fig. 2a), with standardized
384 residuals higher than 2, are excluded from the relationship.
385 Bacteria have developed various adaptation mechanisms to cope with pH variations in the
386 environment, the challenge being to maintain near neutral intracellular pH (Siliakus et al.,

2017 and references therein). Thus, brGDGT-producing bacteria remodel their membrane in response to changing pH by modifying brGDGT cyclisation degree (reflected in the CBT index; Schouten et al., 2013). Similarly, the correlation between RIAN and pH (Eq. 12) supports (i) the effect of pH on the relative distribution of Gram-negative bacterial 3-OH FAs in soils previously observed along Mt. Shennongjia by Wang et al. (2016) and (ii) the fact that the relative abundance of branched homologues vs. straight ones tends to decreases with pH, allowing Gram-negative bacteria to reduce the permeability and fluidity of their membrane. A moderate but significant correlation between RIAN and CBT was also obtained when combining the data from the three mountains (Fig. 2b), consistent with the pH dependence of these two indices.

Despite the potential of the RIAN as a pH proxy, the relatively large amount of scatter of the RIAN-pH relationship has to be taken into account. The RMSE associated with the relationship between RIAN and pH is 0.56, similar to the uncertainty associated with the latest CBT'-pH calibration (RMSE 0.52) developed by De Jonge et al. (2014), even though the latter is based on a larger number of soils (n = 222). Reconstruction of pH using the RIAN-pH calibration (Eq. 12) should therefore be undertaken with special caution (i) in soils with pH < 5, the pH in these soils being significantly overestimated and (ii) in soils with pH >8, where pH is significantly underestimated (Fig. 2c).

3.2.2. RAN_{15} index

Wang et al. (2016) showed the influence of MAAT on the relative abundance of bacterial 3-OH FAs via the calculation of the RAN_{15} index based on *anteiso* and *normal* C_{15} 3-OH FAs. RAN_{15} was negatively correlated with MAAT along Mt. Shennongjia (Wang et al., 2016), leading to the following equations:

$$RAN_{15} = 6.84 - 0.26 \times MAAT \quad (13)$$

412 $MAAT = 17.95 – 1.99 \times RAN_{15}$ ($n = 25$; R^2 0.52; RMSE 2.5 °C; $n_{outliers} = 2$; $p < 0.001$) (14)

413 In the present study, one outlier with standardized residuals higher than 3 was excluded
414 from the relationships between MAAT and RAN_{15} observed along Mt. Shennongjia, slightly
415 modifying the correlations initially published by Wang et al. (2016).

416 RAN_{15} varies in the same range along Mt. Rungwe (1.25 – 5.73), Mt. Majella (0.68 – 6.43)
417 and Mt. Shennongjia (0.68 – 8.09, excluding the outlier; Wang et al., 2016). As previously
418 observed along Mt. Shennongjia (Eqs. 13 and 14; Wang et al., 2016), the RAN_{15} index shows
419 a moderate and negative correlation with MAAT along both Mt. Majella (R^2 0.54) and Mt.
420 Rungwe (R^2 0.70). This is reflected in Eqs. 15 and 16 for Mt. Majella, and Eqs. 17 and 18 for
421 Mt. Rungwe, respectively (Fig. 3a):

422 $RAN_{15} = 5.34 – 0.28 \times MAAT$ (15)

423 $MAAT = 13.54 – 1.94 \times RAN_{15}$ ($n = 11$; R^2 0.52; RMSE 2.9 °C; $p = 0.01$) (16)

424 $RAN_{15} = 8.16 – 0.25 \times MAAT$ (17)

425 $MAAT = 30.50 – 3.19 \times RAN_{15}$ ($n = 28$; R^2 0.52; RMSE 1.6 °C; $p < 0.001$) (18)

426 This shows that MAAT has a similar effect on the distribution of C_{15} 3-OH FAs in soils
427 from different locations, RAN_{15} increasing with decreasing temperature, likely as a result of
428 homeoviscous adaptation. Such a temperature effect was previously reported on the relative
429 distribution of (i) archaeal-derived isoprenoid GDGTs, the number of cyclopentane moieties
430 increasing with temperature (Schouten et al., 2013 and references therein) and of (ii)
431 branched-GDGT, the amount of methyl groups on the carbon chains increasing at low
432 temperatures, enabling the membrane to remain in a liquid crystalline state (Weijers et al.,
433 2007; De Jonge et al., 2014). Similarly, increases in the amount of branched chain fatty acids,
434 saturated fatty acids, long-chain fatty acids and polar carotenoid content were observed in
435 mesophilic and thermophilic bacteria (Siliakus et al., 2017 and references therein). Regarding
436 Gram-negative bacteria, the present results combined with those from Wang et al. (2016)

437 suggest that the relative abundance of *anteiso* vs. *normal* C_{15} 3-OH FA increases with
438 decreasing temperature to maintain membrane fluidity, consistent with the fact that *anteiso*
439 fatty acids have a lower melting point than *normal* ones (Suutari and Lakso, 1994).

440 The correlations between RAN_{15} and MAAT along Mts. Shennongjia, Rungwe and
441 Majella (Fig. 3) do not significantly differ in slope (homogeneity of slope test: df = 2, F =
442 0.072, $p = 0.931$), but display significantly different intercepts (df = 2, F = 22.25, $p < 0.0001$).
443 The present results suggest that regional calibrations with MAAT might be necessary to use
444 RAN_{15} as a temperature proxy. Nevertheless, further application of RAN_{15} to other altitudinal
445 transects distributed worldwide is now needed to confirm this statement.

446 The hydroxy fatty acid profile of Gram-negative bacteria is dependent on environmental
447 conditions but can also greatly vary between genus and even species of bacteria (e.g.
448 *Pseudomonas sp;* Pinkart et al., 1998). Therefore, at a given temperature and independently of
449 other environmental conditions, the ratio of *anteiso* vs. *normal* C_{15} 3-OH FA may strongly
450 vary from one site to another depending on the Gram-negative bacterial communities present
451 in soil. This may notably explain why a given RAN_{15} value corresponds to different MAAT
452 depending on the sampling site. Despite these potential differences in absolute RAN_{15} values
453 between microbial species, the present results suggest that a given range of variation in
454 temperature has the same effect on Gram-negative bacteria whatever the sampling site. In
455 addition, RAN_{15} was shown to be significantly correlated with the MAAT estimates derived
456 from the established GDGT-based proxies (MBT/CBT) along the three investigated
457 mountains (Fig. 3b). This confirms that temperature is the dominant control on RAN_{15} for the
458 three sites.

459

460

461

3.2.3. RAN_{17} index

Similarly to RAN_{15}, RAN_{17}, based on the ratio of *anteiso* and *normal* C_{17} 3-OH FAs, was previously shown to be negatively correlated with MAAT (R^2 0.50) along Mt. Shennongjia (Fig. 4a; Wang et al., 2016). RAN_{17} values are generally lower along Mt. Rungwe (0.33 – 1.62; Table 1) than along Mt. Shennongjia (1.11 – 3.56; Wang et al., 2016) and show high variability along Mt. Majella (0.65 – 4.75; Fig. 4a and Table 1). A significantly negative correlation between RAN_{15} and MAAT is observed along Mt. Rungwe (Fig. 4a), in line with results obtained from Mt. Shennongjia (Wang et al., 2016), leading to the following equations:

$$RAN_{17} = 2.39 - 0.065 \times MAAT \quad (19)$$

$$MAAT = 30.12 - 8.24 \times RAN_{17} \ (n = 28;\ R^2\ 0.54;\ RMSE\ 2.5\ °C;\ p < 0.001) \quad (20)$$

The relationship between RAN_{17} and MAAT along Mt. Majella, expressed in Eqs. 21 and 22, is weaker than the one observed along Mts. Rungwe and Shennongjia and cannot be considered as significant, even though the *p*-value, in the range 0.05-0.10, indicates a trend towards significance:

$$RAN_{17} = 3.16 - 0.15 \times MAAT \quad (21)$$

$$MAAT = 10.80 - 1.84 \times RAN_{17} \ (n = 11;\ R^2\ 0.28;\ RMSE\ 3.8\ °C;\ p = 0.092) \quad (22)$$

The absence of statistical significance in the relationship between RAN_{17} and MAAT is likely due to the high variability of RAN_{17} values along Mt. Majella, leading to a weak correlation. The latter might have several explanations. First, RAN_{17} is weakly (but not significantly) correlated with soil pH (R^2 0.2, $p = 0.16$), in contrast with Mts. Rungwe and Shennongjia, where no correlation between RAN_{17} and pH is observed ($R^2 < 0.020$; data not shown). The alkalinity of Mt. Majella soils (7.8 ± 0.1; Table 1) may lead to a higher influence of pH on RAN_{17}, and in turn, to a higher scattering in the RAN_{17}-MAAT relationship than in

acidic and neutral soils, such as those of Mt. Rungwe (6.1 ± 0.5; Table 1) and Mt. Shennongjia (6.2 ± 1.0; Wang et al., 2016).

Second, it might also not be excluded that precipitation/soil moisture affects 3-OH FA distribution, including RAN_{17} and RAN_{15} indices. Soil moisture is indeed a major factor influencing microbial community structure and characteristics (Brockett et al., 2012). It may therefore affect the diversity of Gram-negative bacteria and thus their membrane lipids, i.e. 3-OH FAs. In the present study RAN_{17} as well as RAN_{15} hint at a linear relationship with MAP along Mt. Majella (R^2 0.28 and R^2 0.54, respectively; data not shown), as also observed along Mt. Shennongjia (R^2 0.48 and R^2 0.50, respectively; Wang et al., 2016). Correlations between RAN_{17}/RAN_{15} and MAP are similar to those observed between these indices and MAAT, as MAAT and MAP strongly co-vary with elevation along both Mt. Majella (R^2 0.93, Supp. Table 2) and Mt. Shennongjia (Wang et al., 2016). Nevertheless, Wang et al. (2016) suggested that MAAT was the dominant parameter influencing RAN_{15} and RAN_{17} along Mt. Shennongjia, as (i) the climate in this region is moist to humid (> 1000 mm/year) making MAP an unlikely limiting ecological factor for the growth of Gram-negative bacteria and (ii) only weak correlations between RAN_{17}/RAN_{15} and punctual soil humidity measurements were observed (R^2 < 0.20; Wang et al., 2016). A similar assumption regarding the predominant influence of MAAT over precipitation/soil humidity on RAN_{15} and RAN_{17} can be made for Mt. Majella, subjected to a moderately humid climate (ca. 800 – 1300 mm precipitation/year; Table 1). Unfortunately, direct soil humidity measurements are not available for Mt. Majella samples and cannot be used to strengthen this hypothesis.

In line with the observations made from the relationships between RAN_{17} and recorded MAAT (Fig. 4a), RAN_{17} is moderately and significantly correlated with brGDGT-derived MAAT estimates along Mts. Rungwe and Shennongjia, whereas no significant correlation is observed along Mt. Majella (Fig. 4b). This may reflect the fact that 3-OH FAs and brGDGTs

511 are produced by different microorganisms, and that the ecological and physiological
512 responses of Gram-negative bacteria and brGDGT-producing bacteria to other environmental
513 factors are not necessarily the same and are site-dependent.

514 In any case, statistical tests revealed no significant differences in either slopes (df = 2, F =
515 1.801, p = 0.174) or in the intercepts of the relationships between RAN_{17} and recorded MAAT
516 along Mts. Rungwe, Majella and Shennongjia (df = 2, F = 0.678, p = 0.512; Fig. 4a). In
517 addition, most data from Mt. Majella fall within the 95 % prediction interval of the RAN_{17}-
518 MAAT correlations along Mts. Rungwe and Shennongjia. This shows that the distribution of
519 Gram-negative bacterial C_{17} 3-OH FAs is similarly affected by temperature variations in soils
520 from different latitudes, with a relative decrease of *normal* vs. *anteiso* homologs with
521 decreasing temperature, as previously observed for C_{15} 3-OH FAs. This suggests that different
522 Gram-negative bacteria species might present the same range of RAN_{17} values at one given
523 temperature, even though microbial diversity can strongly vary from one soil to another,
524 leading to a natural variability of the RAN_{17}.

525 The statistical similarity of the local relationships between RAN_{17} and recorded MAAT
526 along Mts. Rungwe, Majella, and Shennongjia allows the combination of the three datasets,
527 resulting in a significant and moderate negative correlation (Eqs. 23 and 24):

528 $$RAN_{17} = 2.70 - 0.081 \times MAAT \quad (23)$$

529 $$MAAT = 25.74 - 7.38 \times RAN_{17} \ (n = 65;\ R^2\ 0.60;\ RMSE\ 5.1\ °C;\ p = < 0.001) \quad (24)$$

530 This calibration covers a wide range of temperature (ca. 0 – 25 °C; Fig. 4a) and confirms
531 the potential of RAN_{17} as a temperature proxy in terrestrial settings. When combining the data
532 from the three mountains, RAN_{17} also appear to be significantly correlated with brGDGT-
533 derived MAAT (Fig. 4b), consistent with the observations made from recorded MAAT.

534 Even though almost all the data points from Mts. Rungwe, Shennongjia and Majella are
535 within the 95 % prediction interval of the combined calibration (Eq. 24; Fig. 4a), the

substantial uncertainty in temperature reconstruction based on RAN_{17} (RMSE 5.1 °C; Fig. 4c) has to be taken into account, with the largest residuals observed for soils from Mt. Majella, as expected from the high variability of the RAN_{17} values (Fig. 4a). The RMSE of the RAN_{17}-MAAT calibration is similar to that reported for the latest correlation between brGDGT distribution and MAAT (4.6 °C; De Jonge et al., 2014), even though the latter is based on a much larger number of soils (n = 222).

3.3. Implications for the use of 3-OH FAs as environmental proxies

This study espouses the potential of 3-OH FAs as new temperature and pH proxies in soils, in line with the first and recent application of these compounds as paleoproxies in a stalagmite from central China (Wang et al., 2018). Both RAN_{15} and RAN_{17} can be used independently to reconstruct temperature from soils. However, the presently considered data of samples from three different regions suggest that RAN_{15} might only be relevant for temperature reconstructions using independent local calibrations. Analysis of 3-OH FAs in a larger number of soils from over the world is now required to determine to which extent the RIAN, RAN_{15} and RAN_{17} indices can be used as temperature and pH proxies at a global scale.

The remaining scatter in relationships between RIAN and pH (Fig. 2) as well as RAN_{15}/RAN_{17} and MAAT (Figs. 3 and 4) is likely partly due to the intrinsic heterogeneity of soils, and also to variations in the diversity of Gram-negative bacterial communities between soils. Indeed, bacterial community composition, including Gram-negative bacteria, was observed to vary with elevation (Margesin et al., 2008) and 3-OH FA lipid profile is strongly dependent on Gram-negative bacterial species, as previously discussed (e.g. Parker et al., 1982; Bhat and Carlson, 1992).

Additionally, several other factors, such as amount of precipitation/soil moisture, type of vegetation or seasonality, may also have an effect on the relative distribution of 3-OH FAs

562 and thus on RIAN, RAN_{15} and RAN_{17} values in soils. Similar hypotheses are put forward to
563 explain the large uncertainty remaining in global correlations between brGDGT distributions
564 and MAAT (e.g. Peterse et al., 2012) despite recent analytical improvement (De Jonge et al.,
565 2014). Soil humidity (e.g. Dirghangi et al., 2013; Menges et al., 2014) as well as soil type
566 (Davtian et al., 2016) were shown to have an influence on the distribution of brGDGTs in
567 soils. A bias in brGDGT distribution towards the warmest months of the year, when bacterial
568 growth is higher, has also been reported in some soils (e.g. Pautler et al., 2014) and peat
569 (Huguet al., 2013b). More generally, distinct seasonal changes in soil microbial community
570 composition and biomass were previously observed in different settings (e.g. Smit et al.,
571 2001; Habekots et al., 2008; Buckeridge et al., 2013). The specific activity and diversity of
572 Gram-negative bacteria may vary seasonally, leading to preferential production of 3-OH FAs
573 during certain periods of the year.

574 The use of air temperature instead of *in situ* soil temperature could also account for part of
575 the scatter in the RAN_{15} and RAN_{17} correlations, as previously discussed for brGDGT-
576 derived proxies (Weijers et al., 2007; Peterse et al., 2012). As soil temperatures are largely
577 driven by air temperatures, MAAT is assumed to be a good approximation of soil
578 temperature. Nevertheless, an offset may exist between MAAT and soil temperature, as the
579 latter is dependent on numerous factors, such as soil properties (e.g. water content, chemical
580 composition or granulometry), land relief and soil cover (Lehnert, 2014). Soil temperature
581 data may help in partly reducing the scatter in the RAN_{15} and RAN_{17} calibrations. This is
582 hampered by the fact that soil temperatures are much less documented than air temperatures
583 and most of the time not available in the long-term, with only punctual soil temperature
584 measurements when sampling.

585 Additional geochemical and microbiological studies are now necessary to better
586 understand and constrain the influence of environmental parameters on Gram-negative

587 bacterial diversity and 3-OH FA distribution in soils. 3-OH FAs are present in a wide range of
588 terrestrial and aquatic settings, and are likely well preserved in sedimentary archives, as they
589 have been detected in several recent lacustrine sediments (Mendoza et al., 1987; Goosens et
590 al., 1988; Wang et al., 2016), in a Chinese stalagmite spanning the last 9 kyrs (Wang et al.,
591 2018) as well as in a last glacial marine sediment sample from the Baltic Sea and several Late
592 Quaternary sapropels (deposited between 125,000 and 200,000 yrs B.P.; Ten Haven et al.,
593 1987) from the eastern Mediterranean. Therefore, they could be used as paleoenvironmental
594 proxies in various archives, such as paleosols, marine and lacustrine sediments, providing (i) a
595 similar preservation of the C_{10} to C_{18} suite of 3-OH FA homologues and (ii) the development
596 of calibrations specific to each type of environment.
597 Different organic proxies may provide conflicting information, as observed for example in
598 marine environments for alkenone-based $U^{k'}_{37}$ and isoprenoid GDGT-based TEX_{86} (e.g.
599 Lopes dos Santos et al., 2010; McClymont et al., 2012). Independent proxies are therefore
600 required to ensure the reliability of paleoenvironmental reconstructions. Nevertheless, to
601 date, the only organic proxies available for pH and temperature reconstruction in terrestrial
602 environments are those based on brGDGTs. As such, RIAN, RAN_{15} and RAN_{17} may
603 represent independent and complementary temperature and pH proxies to the well-established
604 MBT and CBT indices. In the present study, the pH (Fig. 2b) and temperature (Figs. 3b and
605 4b) proxies derived from 3-OH FAs on the one hand and brGDGTs on the other hand were
606 poorly to moderately correlated and the corresponding relationships were observed to be site-
607 dependent. This may reflect the differences in physiological responses of 3-OH FA- and
608 brGDGT-source microorganisms to environmental changes and/or the variations in microbial
609 community composition along the altitudinal gradients investigated. Such hypotheses remain
610 speculative, as, in contrast with 3-OH FAs, a precise microbial source for brGDGTs has not
611 been identified yet, even though some members of the Gram-negative phylum Acidobacteria

612 may produce these lipids (e.g. Sinninghe Damsté et al., 2018). In any case, the environmental
613 factors impacting 3-OH-FA and brGDGT distribution in soils and the relationships between
614 the temperature and pH proxies derived from these two families of lipids require investigation
615 in a larger set of samples.
616
617 **4. Conclusions**
618
619 The abundance and distribution of 3-OH FAs were determined in surficial soils collected
620 along altitudinal gradients from two different regions – Mt. Rungwe, Tanzania and Mt.
621 Majella, Italy – and were compared with data previously published from Mt. Shennongjia
622 (China; Wang et al., 2016). Gram-negative bacterial 3-OH FAs, with 10 to 18 C, are detected
623 in all soils with even and *normal* chain compounds dominant over even, *iso* and *anteiso*
624 homologs. 3-OH FA distribution is shown to vary with elevation, as reflected in the general
625 decrease in the RIAN, RAN_{15} and RAN_{17} when elevation increases.
626 The combination of data from Mts. Rungwe, Majella and Shennongjia resulted in a
627 significant negative correlation between RIAN and pH, further highlighting the potential of
628 this index as a pH proxy. The correlations between RAN_{15} and MAAT along Mts.
629 Shennongjia, Rungwe and Majella do not significantly differ in slope, suggesting that Gram-
630 negative bacteria respond in the same way to temperature variations in soils from different
631 latitudes, with a relative decrease in *normal* vs. *anteiso* homologs with decreasing
632 temperature. Nevertheless, the relationships between RAN_{15} and MAAT along the three
633 mountains display significantly different intercepts, suggesting that regional calibrations may
634 be required to use RAN_{15} as a temperature proxy. In contrast with RAN_{15}, the statistical
635 similarity of the local relationships between RAN_{17} and MAAT along Mts. Rungwe, Majella,
636 and Shennongjia led to the establishment of a combined calibration covering a wide range of
637 temperature (ca. 0 – 25 °C). Analysis of 3-OH FAs in a large number of soils distributed

worldwide is now required to investigate the applicability of the proxies derived from these lipids at the global scale. As 3-OH FAs are anticipated to be well preserved in sedimentary archives, these compounds should be promising pH and temperature proxies, that would be independent of and complementary to those based on well-established brGDGTs (MBT/CBT). More studies based on natural samples and cultures of Gram-negative bacteria are now needed to better constrain the environmental factors influencing the relative abundance of 3-OH FAs in soils, to investigate the limits and applicability of the RIAN, RAN_{15} and RAN_{17} as paleoproxies and to improve and/or develop the calibrations between these indices and temperature/pH at regional and global scales.

Acknowledgments

This manuscript is dedicated to our colleague and friend Laurent Bergonzini, who passed away in November 2018. We will especially remember his dedication, energy and good spirit while working together. We thank S. Kajula and all the Tanzanians who helped during field sampling. The French EC2CO program (CNRS/INSU) and the Institut Pierre Simon Laplace are thanked for funding. Two anonymous reviewers and the associate editor Paul Greenwood are thanked for their constructive comments which helped to improve the manuscript.

References

Bhat, U.R., Carlson, R.W., 1992. A new method for the analysis of amide-linked hydroxy fatty acids in lipid-As from gram-negative bacteria. Glycobiology 6, 535-539.

Bemigisha, J., Skidmore, A.K., Polce, C., Carranza, J., McCall, M., Prins, H.H.T., 2009. Representation of uncertainty and integration of PGIS-based grazing intensity maps using evidential belief functions. Transactions in GIS 13, 273-293.

663 Bergonzini, L., 1998. Bilans hydrologiques de lacs (Kivu, Tanganyika, Rukwa et Nyassa) du
664 Rift Est-Africain. Muséé Royal de l'Afrique Centrale, Tervuren (Belgique), Annales,
665 Série Sciences Géologiques, vol. 103, p. 183.
666 Bonanomi, G., Gaglione, S.A., Antignani, V., Cesarano, G., 2016. Unimodal pattern of soil
667 hydrophobicity along an altitudinal gradient encompassing Mediterranean, temperate and
668 alpine ecosystems. Plant and Soil 409, 37-47.
669 Brassell, S.C., Eglinton, G., Marlowe I.T., Pflaumann U., Sarnthein M., 1986. Molecular
670 stratigraphy: a new tool for climatic assessment. Nature 320, 129-133.
671 Brockett, B.F.T., Prescott, C.E., Grayston, S.J., 2012. Soil moisture is the major factor
672 influencing microbial community structure and enzyme activities across seven
673 biogeoclimatic zones in western Canada. Soil Biology and Biochemistry 44, 9-20.
674 Buckeridge, K.M., Banerjee, S., Siciliano, S.D., Grogan, P., 2013.The seasonal pattern of soil
675 microbial community structure in mesic low arctic tundra. Soil Biology and Biochemistry
676 65, 338-347.
677 Cheng, J.Y.W., Hui, E.L.C., Lau, A.P.S., 2012. Bioactive and total endotoxins in atmospheric
678 aerosols in the Pearl River Delta region, China. Atmospheric Environment 47, 3-11.
679 Coffinet, S., Huguet, A., Williamson, D., Fosse, C., Derenne, S., 2014. Potential of GDGTs as
680 a temperature proxy along an altitudinal transect at Mount Rungwe (Tanzania). Organic
681 Geochemistry 68, 82-89.
682 Coffinet, S., Huguet, A., Pedentchouk, N., Bergonzini, L., Omuombo, C., Williamson, D.,
683 Anquetil, C., Jones, M., Majule, A., Wagner, T., Derenne, S., 2017. Evaluation of
684 branched GDGTs and leaf wax *n*-alkane δ^2H as (paleo)environmental proxies in East
685 Africa. Geochimica et Cosmochimica Acta 198, 182-193.

686 Davtian, N., Ménot, G., Bard, E., Poulenard, J., Podwojewski, P., 2016. Consideration of soil
687 types for the calibration of molecular proxies for soil pH and temperature using global
688 soil datasets and Vietnamese soil profiles. Organic Geochemistry 101, 140-153.
689 De Jonge, C., Hopmans, E.C., Zell, C.I., Kim, J.H., Schouten, S., Sinninghe Damsté, J.S.,
690 2014. Occurrence and abundance of 6-methyl branched glycerol dialkyl glycerol
691 tetraethers in soils: Implications for palaeoclimate reconstruction. Geochimica et
692 Cosmochimica Acta 141, 97-112.
693 Denich, T.J., Beaudette, L.A., Lee, H., Trevors, J.T., 2003. Effect of selected environmental
694 and physico-chemical factors on bacterial cytoplasmic membranes. Journal of
695 Microbiological Methods 52, 149-182.
696 Dirghangi, S.S., Pagani, M., Hren, M.T., Tipple, B.J., 2013. Distribution of glycerol dialkyl
697 glycerol tetraethers in soils from two environmental transects in the USA. Organic
698 Geochemistry 59, 49–60.
699 Elderfield, H., Ganssen, G., 2000. Past temperature and δ18O of surface ocean waters inferred
700 from foraminiferal Mg/Ca ratios. Nature 405, 442-445.
701 Erez, J., Luz, B., 1983. Experimental paleotemperature equation for planktonic foraminifera.
702 Geochimica et Cosmochimica Acta 47, 1025-1031.
703 Fanin, N., Hättenschwiller, S., Fromin, N., 2014. Litter fingerprint on microbial biomass,
704 activity and community structure in the underlying soil. Plant and Soil 379, 79-91.
705 Habekots, M., Eisenhauer, N., Scheu, S., Steinbeiss, S., Weigelt, A., Gleixner, G., 2008.
706 Seasonal changes in the soil microbial community in a grassland plant diversity gradient
707 four years after establishment. Soil Biology and Biochemistry 40, 2588-2595.
708 Goosens , H., Düren, R.R., De Leeuw, J.W., Schenck, P.A., 1988. Lipids and their mode of
709 occurrence in bacteria and sediments – II. Lipids in the sediment of a stratified,
710 freshwater lake. Organic Geochemistry 14, 27-41.

711 Hazel, J.R., Williams, E.E., 1990. The role of alterations in membrane lipid composition in
712 enabling physiological adaptation of organisms to their physical environment. Progress in
713 Lipid Research 29, 167-227.
714 Hedrick, D.B., Peacock, A.D., Lovley, D.R., Woodard, T.L., Nevin, K.P., Long, P.E., White,
715 D.C., 2009. Polar lipid fatty acids, LPS-hydroxy fatty acids, and respiratory quinones of
716 three Geobacter strains, and variation with electron acceptor. Journal of Industrial
717 Microbiology and Technology 36, 205-209.
718 Huguet, A., Gocke, M., Derenne, S., Fosse, C., Wiesenberg, G.L.B., 2013a. Root-associated
719 branched tetraether source microorganisms may reduce estimated paleotemperatures in
720 subsoil. Chemical Geology 356, 1-10.
721 Huguet, A., Fosse, C., Laggoun-Défarge, F., Delarue, F., Derenne, S., 2013b. Effects of a
722 short-term experimental microclimate warming on the abundance and distribution of
723 branched GDGTs in a French peatland. Geochimica et Cosmochimica Acta 105, 294-315.
724 Huguet, C., Hopmans, E.C., Febo-Ayala, W., Thompson, D.H., Sinninghe Damsté, J.S.,
725 Schouten, S., 2006. An improved method to determine the absolute abundance of
726 glycerol dibiphytanyl glycerol tetraether lipids. Organic Geochemistry 37, 1036–1041.
727 Keinänen, M.M., Korhonen, L.K., Martikainen, P.J., Vartiainen, T., Miettinen, I.T., Lehtola,
728 M.J., Nenonen, K., Pajunen, H., Kontro, M.H., 2003. Gas chromatographic-mass
729 spectrometric detection of 2- and 3-hydroxy fatty acids as methyl esters from soil,
730 sediment and biofilm. Journal of Chromatography B 783, 443-451.
731 Kock, J.L.F., Venter, P., Botha, A., Nigam, S., 1999. Advances in Experimental Medicine and
732 Biology 469, 675-677.
733 Lehnert, M., 2014. Factors affecting soil temperature as limits of spatial interpretation and
734 simulation of soil temperature. Acta Universitatis Palackianae Olomucensis –
735 Geographica 45, 5-21.

736 Lopes dos Santos, R.A., Prange, M., Castañeda, I.S., Schefuß, E., Mulitza, S., Schulz, M.,
737 Niedermeyer, E.M., Sinninghe Damsté, J.S., Schouten, S., 2010. Glacial–interglacial
738 variability in Atlantic meridional overturning circulation and thermocline adjustments in
739 the tropical North Atlantic. Earth and Planetary Science Letters 300, 407–414.
740 Margesin, R., Jud, M., Tscherko, D., Schinner, F., 2008. Microbial communities and activities
741 in alpine and subalpine soils. FEMS Microbiology Ecology 67, 208-218.
742 McClymont, E.L., Ganeshram, R.S., Pichevin, L.E., Talbot, E.M., van Dongen, B.E., Thunell,
743 R.C., Haywood, A.M., Singarayer, J.S., Valdes, P.J., 2012. Sea-surface temperature
744 records of Termination 1 in the Gulf of California: challenges for seasonal and
745 interannual analogues of tropical Pacific climate change. Paleoceanography 27, PA2202.
746 Mendoza Y.A., Gülaçar F.O., Buchs A., 1987. Comparison of extraction techniques for bound
747 carboxylic acids in recent sediments. 2. β-hydroxyacids. Chemical Geology 62, 321-330.
748 Menges, J., Huguet, C., Alcañiz, J.M., Fietz, S., Sachse, D., Rosell-Melé, A., 2014. Water
749 availability determines branched glycerol dialkyl glycerol tetraether distributions in soils
750 of the Iberian Peninsula. Biogeosciences 11, 2571-2581.
751 Miyagawa, E., Azuma, R., Suto, T., 1979. Cellular fatty acid composition in Gram-negative
752 obligately anaerobic rods. Journal of General and Applied Microbiology 25, 41-51.
753 Nemergut, D.R., Cleveland C.C., Wieder W.R., Washenberger, C.L., Townsend, A.R., 2010.
754 Plot-scale manipulations of organic matter inputs to soils correlate with shifts in
755 microbial community composition in a lowland tropical rain forest. Soil Biology and
756 Biochemistry 42, 2153–2160.
757 Oyaizu, H., Komagata, K., 1983. Grouping of Pseudomonas species on the basis of cellular
758 fatty acid composition and the quinone system with special reference to the existence of
759 3-hydroxy fatty acids. Journal of General and Applied Microbiology 29, 17-40.

760 Parker, J.H., Smith, G.A., Fredrickson, H.L., Vestal, J.R., White, D.C., 1982. Sensitive assay,
761 based on hydroxy fatty acids from lipopolysaccharide lipid A, from Gram-negative
762 bacteria in sediments. Applied and Environmental Microbiology 44, 1170-1177.
763 Pautler, B. G., Reichart, G.J., Sanborn, P.T., Simpson, M.J., Weijers, J.W.H., 2014.
764 Comparison of soil derived tetraether membrane lipid distributions and plant-wax δD
765 compositions for reconstruction of Canadian Arctic temperatures. Palaeogeography,
766 Palaeoclimatology, Palaeoecology 404, 78-88.
767 Peterse, F., van der Meer, J., Schouten, S., Weijers, J.W.H., Fierer, N., Jackson, R.B., Kim, J.-
768 K., Sinninghe Damsté, J.S., 2012. Revised calibration of the MBT–CBT
769 paleotemperature proxy based on branched tetraether membrane lipids in surface soils.
770 Geochimica et Cosmochimica Acta 96, 215-229.
771 Peterse, F., Martínez-García, A., Zhou, B., Beets, C.J., Princs, M.A., Zheng, H., Eglinton,
772 T.I., 2014. Molecular records of continental air temperature and monsoon precipitation
773 variability in East Asia spanning the past 130,000 years. Quaternary Science Reviews 83,
774 76-82.
775 Pinkart, H.C., White, D.C., 1998. Lipids of Pseudomonas. In: Montie, T.C (Ed.),
776 Biotechnology Handbooks.Springer Science, New York, pp. 111-138.
777 Prado, A., Da Costa M.S., Madeira V.M., 1988. Effect of growth temperature on the lipid
778 composition of two strains of Thermus sp. Journal of General Microbiology 134, 1653-
779 1660.
780 Raetz C.R.H, Reynolds C.M., Trent M.S., Bishop R.E., 2007. Lipid A modification systems
781 in Gram-negative bacteria. Annual Review of Biochemistry 76, 295-329
782 Saraf, A., Larsson, L., Bruge, H., Milton, D., 1997. Quantification of ergostreol and 3-
783 hydroxy fatty acids in settled house dust by gas chromatography-mass spectrometry:

784 comparison with fungal culture and determination of endotoxin by a Limulus amebocyte
785 lysate assay. Applied and Environmental Microbiology 63, 2554-2559.
786 Schouten, S., Hopmans, E.C., Sinninghe Damsté, J.S., 2013. The organic geochemistry of
787 glycerol dialkyl glycerol tetraethers: a review. Organic Geochemistry 54, 19-61.
788 Siliakus, M.F., van der Oost, J., Kengen, S.W.M., 2017. Adaptations of archaeal and bacterial
789 membranes to variations in temperature, pH and pressure. Extremophiles 21, 651-670.
790 Sinensky M. (1974). Homeoviscous adaptation - a homeostatic process that regulates the
791 viscosity of membrane lipids in *Escherichia coli*. Proceedings of the National Academy
792 of Sciences of the United States of America 71, 522–525.
793 Sinninghe Damsté, J.S., Rijpstra, W.I., Hopmans, E.C., Weijers, J.W.H., Foesel, B.U.,
794 Overmann, J., Dedysh, S.N., 2011. 13,16-dimethyl octacosanedioic acid (iso-diabolic
795 acid), a common membrane-spanning lipid of Acidobacteria subdivisions 1 and 3.
796 Applied and Environmental Microbiology 77, 4147-4154.
797 Sinninghe Damsté, J.S., Rijpstra, W.I.C., Hopmans, E.C., Foesel, B.U., Wüst, P.K.,
798 Overmann, J., Tank, M., Bryant, D.A., Dunfield, P.F., Houghton, K., Stott, M., 2014.
799 Ether- and ester-bound iso-diabolic acid and other lipids in members of Acidobacteria
800 Subdivision 4. Applied and Environmental Microbiology 80, 5207-5218.
801 Sinninghe Damsté, J.S., Rijpstra, I.C., Foesel, B.U., Huber, K.J., Overmann, J., Nakagawa, S.,
802 Kim, J.J., Dunfield, P.F., Dedysh, S.N., Villanueva, L., 2018. An overview of the
803 occurrence of ether- and ester-linked iso-diabolic acid membrane lipids in microbial
804 cultures of the Acidobacteria: Implications for brGDGT paleoproxies for temperature and
805 pH. Organic Geochemistry 124, 63-76.

Smit E., Leeflang P., Gommans, S., van den Broek, J., van Mil, S., Wernars, K., 2001. Diversity and Seasonal Fluctuations of the Dominant Members of the Bacterial Soil Community in a Wheat Field as Determined by Cultivation and Molecular Methods. Applied and Environmental Microbiology 67, 2284-2291.

Stanisci, A., Pelino, G., Blasi, C. (2005). Vascular plant diversity and climate change in the alpine belt of the central Apennines (Italy). Biodiversity and Conservation 14, 1301–1318.

Suutari, M., Laakso, S., 1992. Changes in fatty acid branching and unsaturation of Streptomyces griseus and Brevibacterium fermentans as a response to growth temperature. Applied and Environmental Microbiology 28, 2338-2340.

Suutari, M., Laakso, S., 1994. Microbial fatty acids and thermal adaptation. Critical Reviews in Microbiology 20, 285–328.

Ten Haven, H.L., Baas, M., De Leeuw, J.W., Schenck, P.A., 1987. Late Quaternary Mediterranean sapropels, I – On the origin of organic matter is sapropel S7. Marine Geology 75, 137-156.

Tilumanywa, V.T., 2013. Land use and livelihood changes in the Mount Rungwe ecosystem, Tanzania. PhD thesis, Stellenbosh University, 273. http://scholar.sun.ac.za/handle/10019.1/85786

Tyagi, P., Yamamoto, S., Kawamura, K., 2015. Hydroxy fatty acids in fresh snow samples from northern Japan: long-range atmospheric transport of Gram-negative bacteria by Asian winter monsoon. Biogeosciences 12, 7071-7080.

Volkman, J.K., Barrett, S.M., Blackburn, S.J., 1999. Fatty acids and hydroxy fatty acids in three species of freshwater eustigmatophytes. Journal of Phycology 35, 1005-1012.

Wakeham, S.G., 1999. Monocarboxylic, dicarboxylic and hydroxy acids released by sequential treatments of suspended particles and sediments of the Black Sea. Organic Geochemistry 30, 1059-1074.

831 Wakeham, S.G., Pease, T.K., Benner, R., 2003. Hydroxy fatty acids in marine dissolved
832 organic matter as indicators of bacterial membrane material. Organic Geochemistry 34,
833 857-868.
834 Wang, C., Zhang, H., Huang, X., Huang, J., Xie, S., 2012. Optimization of acid digestion
835 conditions on the extraction of fatty acids from stalagmites. Frontiers of Earth Science 6,
836 109–114.
837 Wang, C., Bendle, J., Yang, Y., Yang, H., Sun, H., Huang, J., Xie, S., 2016. Impacts of pH
838 and temperature on soil bacterial 3-hydroxy fatty acids: Development of novel terrestrial
839 proxies. Organic Geochemistry 94, 21-31.
840 Wang, C., Bendle, J., Zhang, H., Yang, Y., Liu, D., Huang, J., Cui, J., Xie, S., 2018. Holocene
841 temperature and hydrological changes reconstructed by bacterial 3-hydroxy fatty acids in
842 a stalagmite from Central China. Quaternary Science Reviews 192, 97-105.
843 Weijers, J.W.H., Schouten, S., van den Donker, J.C., Hopmans, E.C., Sinninghe Damsté, J.S.,
844 2007. Environmental controls on bacterial tetraether membrane lipid distribution in soils.
845 Geochimica et Cosmochimica Acta 71, 703-713.
846 Wilkinson, S.G., 1988. Gram-negative bacteria. In: Ratledge C., Wilkinson S.G. (Eds),
847 Microbial Lipids, vol. 1. Academic Press, New York, pp. 199-488.
848 Williamson, D., Majule, A., Delalande, M., Mwakisunga, B., Mathé, P.-E., Gwambene, B.,
849 Bergonzini, L., 2014. A potential feedback between land use and climate in the Rungwe
850 tropical highland stresses a critical environmental research challenge. Current Opinion in
851 Environmental Sustainability 6, 116-122.
852 Yang, H., Xiao, W., Jia, C., Xie, S., 2014. Paleoaltimetry proxies based on bacterial branched
853 tetraether membrane lipids in soils. Frontiers of Earth Science 9, 13–25.

Yang, H., Lü, X., Ding, W., Lei, Y., Dang, X., Xie, S., 2015. The 6-methyl branched tetraethers significantly affect the performance of the methylation index (MBT′) in soils from an altitudinal transect at Mount Shennongjia. Organic Geochemistry 82, 42-53.

Yang, Y., Wang, C., Zhang, H., Huang, J., Xie, S., 2016. Influence of extraction methods on the distribution pattern and concentration of fatty acids and hydroxy fatty acids in soil samples: Acid digestion versus saponification. Geochemical Journal 50, 439-443.

Zelles, L., Bai, Q.Y., Rackwitz, R., Chadwick, D., Beese, F., 1995. Determination of phospholipid- and lipopolysaccharide-derivedfatty acids as an estimate of microbial biomass and community structures in soils. Biology and Fertility of Soils 19, 115-123.

Zelles, L., 19997. Phospholipid fatty acid profiles in selected members of soil microbial communities. Chemosphere 35, 275-294.

Zelles, L., 1999. Fatty acid patterns of phospholipids and polysaccharides in the characterization of microbial communities in soil: a review. Biology and Fertility of Soils 29, 111-129.

Zheng, Y., Li, Q., Wang, Z., Naafs, B.D.A., Yu, X., Pancost, R.D. 2015. Peatland GDGT records of Holocene climatic and biogeochemical responses to the Asian Monsoon. Organic Geochemistry 87, 86-95.

Figure and table captions

Figure 1. ~~Extracted~~ Ion mass (*m/z* 175) chromatogram showing distribution of 3-OH FAs in sample 1 (520 m altitude) from Mt. Rungwe. *Normal*, *iso* and *anteiso* 3-OH FAs are represented by red circles, green triangles and blue squares, respectively.

Figure 2. (a) Relationship between RIAN and soil pH along Mt. Rungwe and Mt. Majella (this study) and Mt. Shennongjia (Wang et al., 2016). Data for Mt. Rungwe samples are in blue, those for Mt. Majella in green and those from Mt. Shennongjia in orange. Black dashed line represents correlation based on combined data from the three mountains. Dotted lines represent 95% prediction interval for the combined correlation. The empty symbols are outliers as defined in the text. ~~**(b)** Offset between the measured and calculated pH values based on Eq. 6 plotted versus measured pH values. Symbols are the same as those used in panel (a).~~ **(b)** Relationship between RIAN and CBT along Mt. Rungwe and Mt. Majella (this study) and Mt. Shennongjia (Wang et al., 2016). Black dashed line represents correlation based on combined data from the three mountains. **(c)** Offset between the measured and calculated pH values based on Eq. 12 plotted versus measured pH values Symbols in ~~panels~~ **(b)** and **(c)** are the same as those used in ~~panel~~ **(a).**

Figure 3. **(a)** Relationship between RAN_{15} and mean annual air temperature (MAAT) along Mt. Rungwe and Mt. Majella (this study) and Mt. Shennongjia (Wang et al., 2016). Data and correlations for Mt. Rungwe samples are in blue, those for Mt. Majella in green and those from Mt. Shennongjia in orange. Dotted lines represent 95% prediction interval for each local correlation. The empty symbols are outliers as defined in the text. **(b)** Relationship between RAN_{15} and brGDGT-derived MAAT estimates along Mt. Rungwe and Mt. Majella (this study) and Mt. Shennongjia (Wang et al., 2016). BrGDGT-derived MAAT estimates for soils from Mts. Rungwe and Shennongjia were obtained using local soil calibrations developed by Coffinet et al. (2017) and Yang et al. (2015), respectively, whereas the global soil calibration by De Jonge et al. (2014) was applied to soils from Mt. Majella. Symbols are the same as those used in panel **(a).**

Figure 4. (a) Relationship between RAN_{17} and MAAT along Mt. Rungwe and Mt. Majella (this study) and Mt. Shennongjia (Wang et al., 2016). Data and correlations for Mt. Rungwe samples are in blue, those for Mt. Majella in green and those for Mt. Shennongjia in orange. Black dashed line represents correlation based on combined data from the three mountains. Dotted lines represent 95% prediction interval for local and global correlations. ~~**(b)** Offset between the measured and calculated MAAT values based on Eq. 17 plotted versus measured MAAT values.~~ **(b)** Relationship between RAN_{17} and brGDGT-derived MAAT estimates along Mt. Rungwe and Mt. Majella (this study) and Mt. Shennongjia (Wang et al., 2016). BrGDGT-derived MAAT estimates for soils from Mts. Rungwe and Shennongjia were obtained using local soil calibrations developed by Coffinet et al. (2017) and Yang et al. (2015), respectively, whereas the global soil calibration by De Jonge et al. (2014) was applied to soils from Mt. Majella. Black dashed line represents correlation based on combined data from the three mountains. **(c)** Offset between the measured and calculated MAAT values based on Eq. 24 plotted versus measured MAAT values. Symbols in panels **(b)** and **(c)** are the same as those used in panel **(a).**
~~Symbols are the same as those used in panel (a).~~

Mis en forme : Police :Gras
Mis en forme : Police :Gras
Mis en forme : Police :Gras
Mis en forme : Police :Gras
Mis en forme : Police :Gras
Mis en forme : Police :Gras
Mis en forme : Police :Gras
Mis en forme : Police :Gras
Mis en forme : Police :Gras

~~**Figure 5.** Relationships between (a) RAN_{15} and brGDGT derived MAAT estimates, (b) RAN_{17} and brGDGT derived MAAT estimates and (c) RIAN and CBT along Mt. Rungwe and Mt. Majella (this study) and Mt. Shennongjia (Wang et al., 2016). Data and correlations for Mt. Rungwe samples are in blue, those for Mt. Majella in green and those for Mt. Shennongjia in orange. BrGDGT derived MAAT estimates for soils from Mts. Rungwe and Shennongjia were obtained using local soil calibrations developed by Coffinet et al. (2017) and Yang et al. (2015), respectively, whereas the global soil calibration by De Jonge et al. (2014) was applied to soils from Mt. Majella.~~

Table 1. Location and bulk features of soil samples from Mt. Rungwe and Mt. Majella collected in 2012 and 2016, abundance and distribution of 3-OH FAs plus indices derived from them as well. n.a., not available.

Supplementary Table 1. Mean annual precipitation (MAP) recorded along Mt. Majella.

Supplementary Table 2. Relative abundances (%) and total concentration (µg/g dry soil) of the *normal, iso* and *anteiso* 3-OH FAs in soils from Mt. Rungwe and Mt. Majella (n.d., not detected).

Supplementary Table 3. Indices derived from brGDGTs for soils from Mt. Majella and MAAT estimates calculated using the global soil calibration by De Jonge et al. (2014).
~~**Supplementary Table 3.** Indices derived from brGDGTs for soils from Mt. Majella and MAAT estimates calculated using the global soil calibration by De Jonge et al. (2014).~~

Mis en forme : Justifié

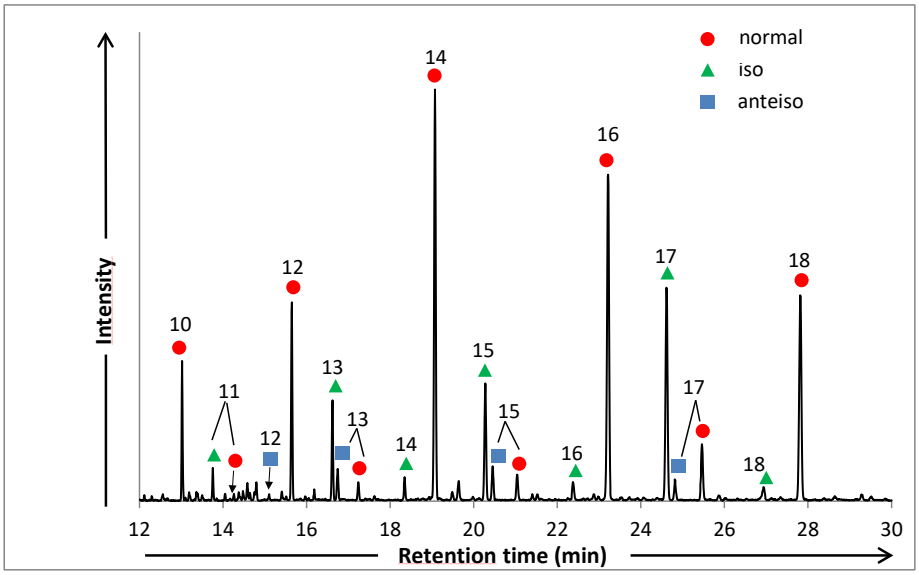
normal
iso
anteiso
Intensity
Retention time (min)
12
14
16
18
20
22
24
26
28
30
10
11
12
13
13
14
15
15
16
17
17
18
18

Fig. 1

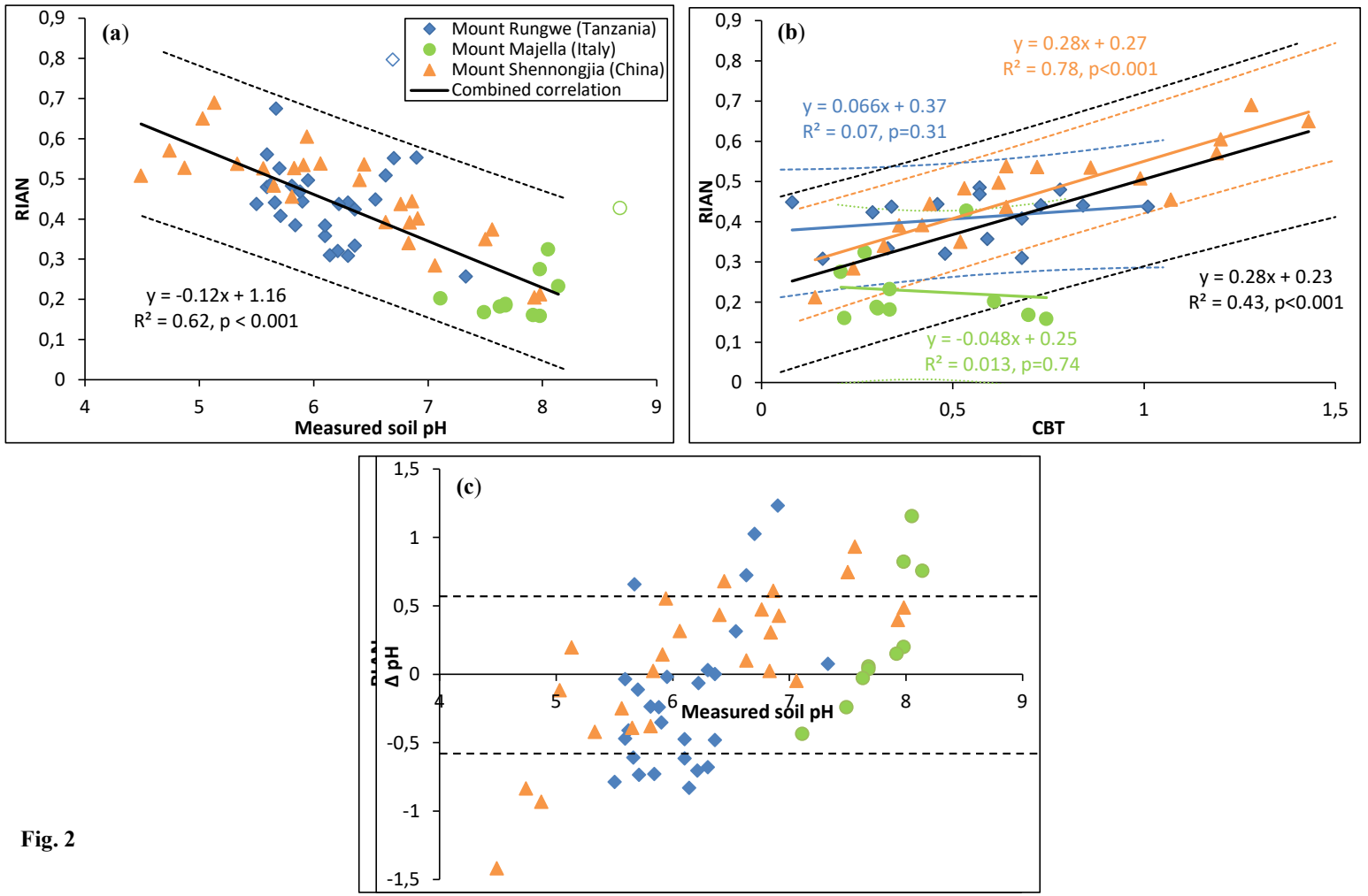
(a)
Mount Rungwe (Tanzania)
Mount Majella (Italy)
Mount Shennongjia (China)
Combined correlation
y = -0.12x + 1.16
R² = 0.62, p < 0.001
RIAN
Measured soil pH
(b)
y = 0.28x + 0.27
R² = 0.78, p<0.001
y = 0.066x + 0.37
R² = 0.07, p=0.31
y = 0.28x + 0.23
R² = 0.43, p<0.001
y = -0.048x + 0.25
R² = 0.013, p=0.74
RIAN
CBT
(c)
Δ pH
Measured soil pH

Fig. 2

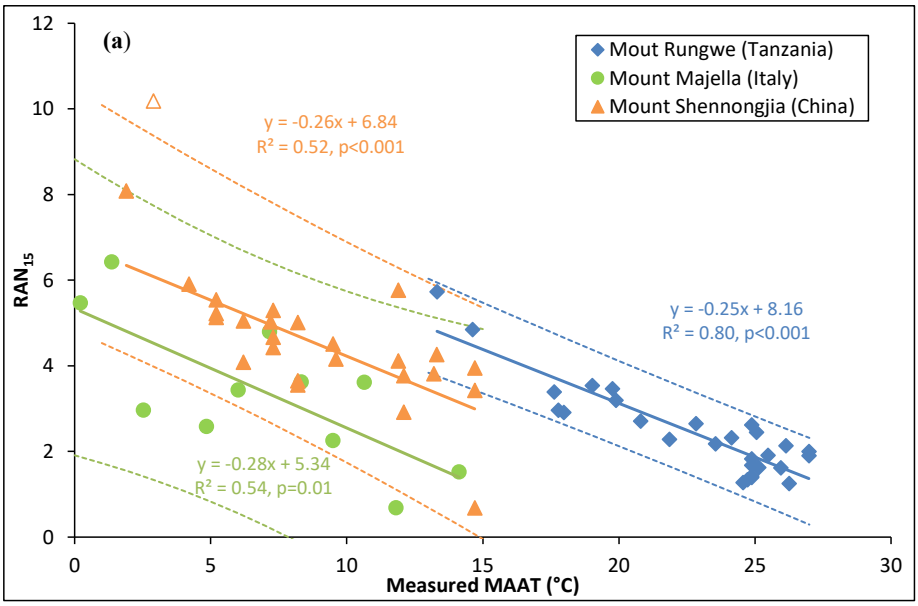

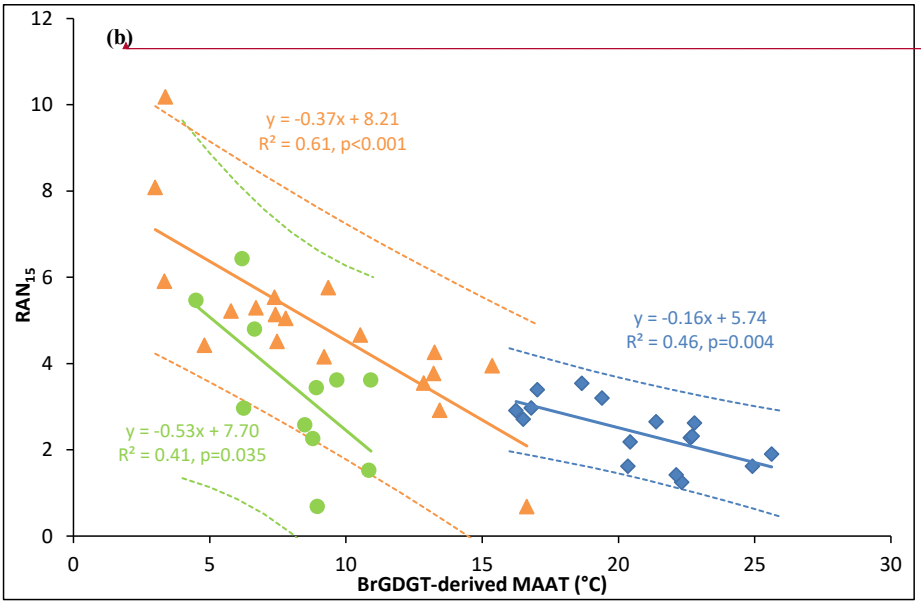

Mis en forme : Police :Gras

Fig. 3

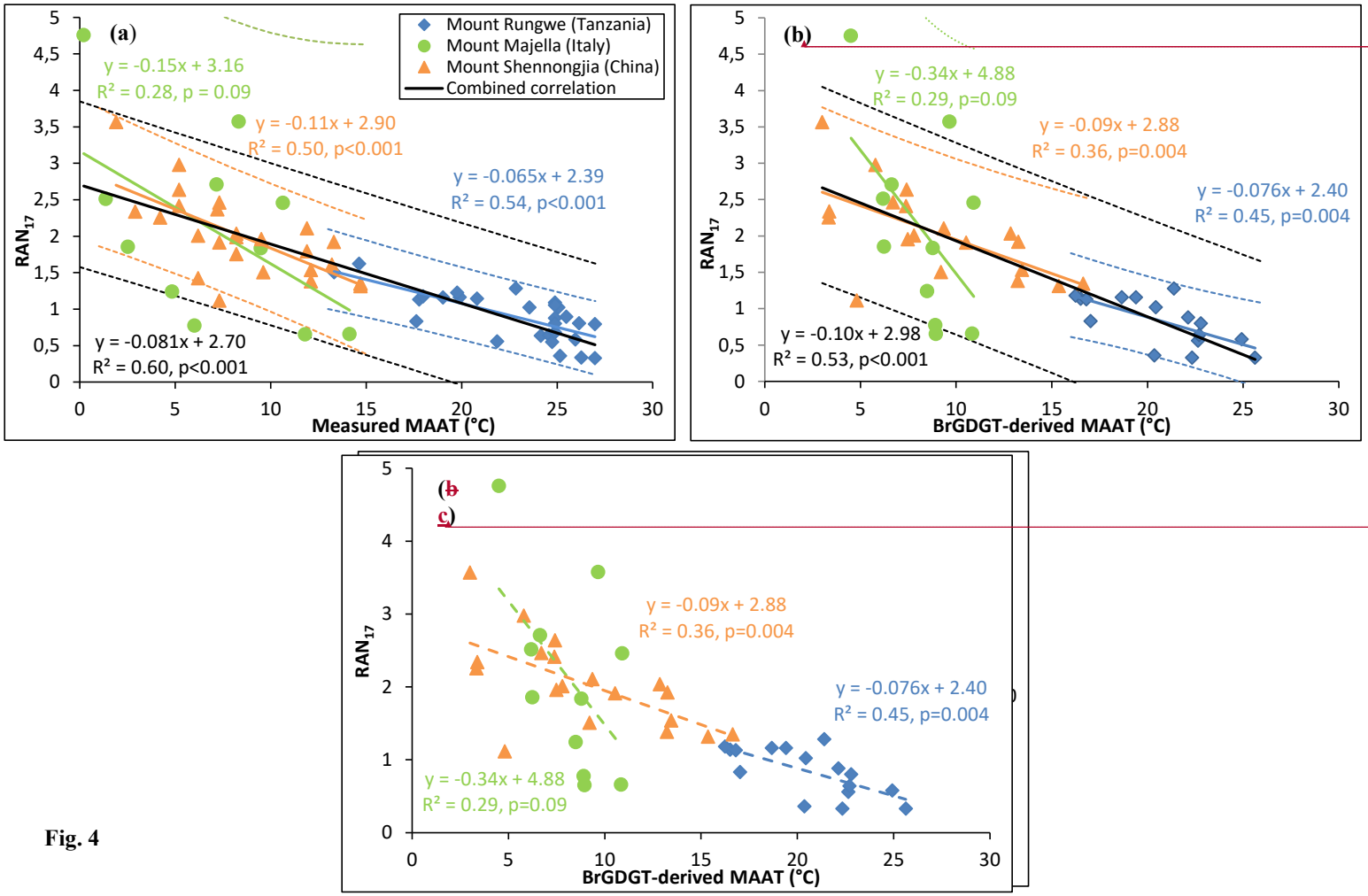

Fig. 4

Mis en forme : Police :Gras

Mis en forme : Police :Gras

Table 1

Campaign	Sample	Altitude (m)	Coordinates	MAAT[a] (°C)	MAP[b] (mm/year)	Soil pH	Corg (%)	Total 3-OH FAs (μg/g C_{org})	RIAN	RAN_{15}	RAN_{17}
Mt. Rungwe (2012)	1	520	S 09.40492° E 33.90782°	25.7	n.a.	6.5	4.9	314.9	0.45	1.90	0.33
	2	520	S 09.40450° E33.90870°	25.7	n.a.	5.6	1.5	77.3	0.56	2.00	0.79
	3	640	S 09.37025° E 33.79949°	24.8	n.a.	6.4	6.2	344.2	0.42	1.25	0.33
	4	660	S 09.22000° E 33.47000°	24.7	n.a.	6.1	5.2	79.8	0.38	2.14	0.81
	5	692	S 09.35699° E 33.79721°	24.4	n.a.	6.3	2.6	105.8	0.31	1.62	0.58
	6	826	S 09.35270° E 33.82296°	23.4	n.a.	5.9	5.8	205.7	0.44	1.62	0.36
	7	840	S 09.35150° E33.82280°	23.3	n.a.	5.8	5.6	56.4	0.38	2.45	1.02
	8	869	S 09.33512° E 33.76300°	23.1	n.a.	5.9	5.2	28.7	0.50	1.83	1.05
	9	869	S 09.33008° E 33.75884°	23.1	n.a.	7.3	4.8	64.2	0.26	1.42	0.88
	10	869	S 09.33640° E 33.75590°	23.1	n.a.	6.2	7.1	17.9	0.32	1.68	1.09
	11	869	S 09.33008° E 33.75884°	23.1	n.a.	6.1	4.4	25.5	0.31	2.62	0.80
	12	994	S 09.33470° E 33.81031°	22.2	n.a.	6.4	3.6	191.4	0.33	2.32	0.64
	13	1092	S 09.32068° E 33.80958°	21.5	n.a.	6.1	2.3	141.3	0.36	2.18	1.02
	14	1211	S 09.30013° E 33.80783°	20.6	n.a.	5.7	8	96.8	0.44	2.65	1.28
	15	1374	S 09.28262° E 33.81349°	19.4	n.a.	5.6	6.3	116.0	0.48	2.28	0.56
	16	1550	S 09.26021° E 33.82095°	18.2	n.a.	5.5	4.9	260.0	0.44	2.71	1.14
	17	1702	S 09.35993° E 33.81637°	17.1	n.a.	5.7	2.9	226.9	0.41	3.20	1.16
	18	1846	S 09.22716° E 33.81249°	16.0	n.a.	5.6	3.2	111.3	0.49	3.54	1.16
	19	2020	S 09.02202° E 33.56576°	14.7	n.a.	5.9	2.5	580.4	0.47	2.91	1.18
	20	2055	S 09.02124° E 33.56478°	14.5	n.a.	6.2	5.3	458.1	0.44	2.97	1.13
	21	2080	S 09.07322° E 33.40782°	14.3	n.a.	6.3	0.8	1062.5	0.44	3.39	0.83
Mt. Rungwe (2016)	22	770	S 09.28966° E 33.90248°	23.9	n.a.	7.3	5.2	121.3	0.33	1.89	0.88
	23	870	S 09.33512° E 33.76305°	23.1	n.a.	6.7	2.7	270.7	0.49	1.39	0.45
	24	895	S 09.33646° E 33.75608°	22.9	n.a.	6.6	7.1	123.7	0.51	1.34	0.55
	25	923	S 09.33295° E 33.75195°	22.7	n.a.	6.7	3.6	193.1	0.80	1.27	0.64
	26	1723	S 09.12449° E 33.83101°	16.9	n.a.	5.8	3.3	79.7	0.48	3.46	1.23
	27	2580	S 09.03545° E 33.77150°	10.6	n.a.	6.9	16.7	52.4	0.55	4.84	1.62
	28	2797	S 09.02571° E 33.78635°	9.1	n.a.	5.7	9.3	121.6	0.53	5.73	1.50
Mt. Majella (2016)	29	400	N 42.08696° E 14.20067°	14.1	789	8.1	18.5	14.5	0.32	1.52	0.65
	30	800	N 42.08391° E 14.17626°	11.8	882	8.7	30.2	6.9	0.43	0.68	0.65
	31	1000	N 42.07850° E 14.16762°	10.6	929	7.7	18.3	103.9	0.19	3.61	2.46
	32	1200	N 42.07572° E 14.1628°	9.5	976	7.7	28.0	62.9	0.18	2.25	1.83
	33	1400	N 42.07427° E 14.15488°	8.3	1022	7.6	28.6	49.8	0.18	3.62	3.57
	34	1600	N 42.07617° E 14.14216°	7.2	1069	7.1	38.6	22.4	0.20	4.79	2.71
	35	1800	N 42.07965° E 14.13433°	6.0	1116	8.0	42.3	2.3	0.16	3.43	0.77
	36	2000	N 42.08598° E 14.12597°	4.8	1162	8.1	37.3	2.1	0.23	2.58	1.24
	37	2400	N 42.09066° E 14.09672°	2.5	1256	7.5	36.7	32.8	0.17	2.96	1.85
	38	2600	N 42.08882° E 14.08881°	1.4	1303	8.0	16.2	92.0	0.27	6.43	2.51
	39	2800	N 42.08780° E 14.0867°	0.2	1350	7.9	24.8	85.8	0.16	5.46	4.75

[a]Calculated based from climatic data available from 3 meteorological stations along Mt. Rungwe and Mt. Majella (cf. Section 2).
[b]Extrapolated from precipitation data available along Mt. Majella (cf. Supp. Table 1).

Supplementary Table 1. Mean annual precipitation (MAP) recorded along Mt. Majella.

Altitude (m)	MAP (mm/year)
325	813
650	779
767	973
1000	898
1251	928
1500	1035
2000	1163
2500	1291
2800	1368

Supplementary Table 2. Relative abundances (%) and total concentration (µg/g dry soil) of the normal, iso and anteiso 3-OH FAs in soils from Mt. Rungwe and Mt. Majella (n.d., not detected).

Campaign	Sampling month	Sample	Altitude	*n*- C10	*iso*- C11	*anteiso*- C11	*n* -C11	*anteiso* -C12	*n*- C12	*iso* -C13	*anteiso* -C13	*n*- C13	*iso* -C14	*n*- C14	*iso* -C15	*anteiso* -C15	*n*- C15	*iso* -C16	*n*- C16	*iso* -C17	*anteiso* -C17	*n*- C17	iso-C18	*n*- C18	Concentration (µg/g soil)
	April	1	520	2,73	0,48	0,08	0,19	0,16	6,44	3,97	0,58	0,57	1,12	19,79	5,20	2,11	1,11	1,08	21,31	9,48	1,26	3,85	0,75	17,76	15,43
	April	2	520	0,44	n.d.	n.d.	n.d.	n.d.	4,68	2,31	0,29	0,35	0,86	27,68	5,71	2,03	1,01	1,77	19,38	10,59	1,34	1,69	1,05	18,81	1,16
	April	3	640	3,97	0,95	0,04	0,23	0,22	7,06	3,64	1,33	0,77	1,02	19,64	5,84	1,62	1,30	0,99	19,74	12,65	1,15	3,44	0,99	13,43	21,34
	December	4	660	2,09	0,52	0,02	0,19	0,16	5,50	3,35	0,53	0,64	1,14	22,19	6,51	2,17	1,02	1,32	22,55	11,34	1,30	1,61	0,89	14,98	4,15
	April	5	692	2,28	0,92	0,05	0,22	0,15	5,74	3,18	0,97	0,63	1,11	21,71	8,14	1,99	1,23	1,62	20,10	12,12	1,55	2,66	1,17	12,46	2,75
	December	6	826	3,31	0,64	0,09	0,26	0,18	7,10	4,14	0,66	0,71	1,12	19,92	5,23	2,07	1,27	1,07	20,53	9,34	1,32	3,69	0,62	16,75	11,93
	April	7	840	5,96	1,33	0,07	0,40	0,30	10,14	4,80	1,39	0,82	1,49	31,41	7,79	2,98	1,22	1,28	22,34	12,90	1,63	1,60	1,37	16,61	3,16
	April	8	869	2,02	0,93	0,05	0,34	n.d.	6,66	2,88	0,87	0,90	1,02	29,16	5,89	1,83	1,00	0,91	18,39	8,62	1,40	1,32	n.d.	15,80	1,49
	April	9	869	1,80	0,71	0,08	0,20	0,37	4,74	2,46	2,16	0,67	1,25	21,17	8,56	1,92	1,35	1,86	20,03	13,25	1,83	2,09	1,18	12,32	3,08
	April	10	869	1,95	0,55	0,09	0,20	0,23	5,97	3,65	0,63	1,21	1,42	22,91	7,42	2,27	1,35	1,63	19,18	12,07	1,62	1,48	0,76	13,40	1,27
Mt. Rungwe (2012)	April	11	869	0,84	0,50	0,03	0,19	0,34	5,27	3,55	1,03	0,72	1,77	29,00	9,30	3,27	1,25	1,35	19,22	8,70	1,05	1,31	1,99	9,33	1,12
	April	12	994	2,00	0,52	0,04	0,21	0,26	6,61	4,02	0,93	0,64	1,47	20,98	6,67	2,58	1,11	1,31	20,69	11,92	1,24	1,95	0,70	14,13	6,89
	April	13	1092	6,05	2,06	0,17	0,59	0,43	10,51	5,22	0,87	0,72	1,20	23,67	6,18	2,07	0,95	1,17	17,06	9,56	1,32	1,29	0,25	8,64	3,25
	April	14	1211	8,91	0,80	0,04	0,36	0,23	8,88	2,89	1,59	0,74	1,20	24,46	5,51	2,32	0,87	1,10	15,78	7,96	1,68	1,31	1,27	12,09	7,74
	April	15	1374	6,74	0,50	n.d.	0,25	0,59	8,22	5,07	1,71	0,79	1,75	21,28	4,07	2,20	0,96	1,02	18,88	6,24	1,04	1,86	0,71	16,13	7,31
	April	16	1550	3,69	0,57	0,04	0,24	0,18	9,05	3,03	1,04	0,65	1,17	22,90	5,05	2,26	0,83	1,24	19,14	9,62	1,35	1,18	1,21	15,55	12,74
	April	17	1702	4,53	0,70	0,07	0,26	0,21	8,70	3,33	0,69	0,55	1,31	20,85	6,05	2,83	0,89	1,06	17,64	9,89	1,50	1,29	0,48	17,18	6,58
	April	18	1846	3,78	0,49	0,06	0,20	0,19	10,58	3,34	0,73	0,67	1,41	23,86	4,92	2,93	0,83	0,95	18,70	7,80	1,40	1,20	0,42	15,53	3,56
	April	19	2020	3,59	0,39	0,05	0,22	0,12	9,51	3,81	0,65	0,63	1,31	23,52	5,67	2,70	0,93	0,93	19,33	7,82	1,40	1,19	0,53	15,70	14,51
	April	20	2055	3,24	0,41	0,07	0,19	0,14	9,02	3,72	0,71	0,61	1,46	23,41	5,25	2,75	0,93	0,96	19,07	9,20	1,40	1,23	0,68	15,56	24,28
	December	21	2080	2,01	0,22	0,03	0,16	0,15	6,41	2,59	1,46	0,68	1,43	19,76	4,75	3,41	1,01	1,06	20,19	9,20	1,46	1,76	0,83	21,41	8,50
		22	770	2,86	0,49	0,06	0,11	0,10	5,15	2,71	0,44	0,54	0,99	18,48	5,89	1,78	0,94	1,07	20,71	15,60	1,67	1,91	1,11	17,39	6,31
		23	870	5,76	0,69	0,08	0,35	0,19	6,43	2,46	0,37	0,79	0,69	19,74	4,48	1,50	1,44	1,26	16,39	9,35	1,20	1,72	0,97	24,12	7,31
		24	895	7,11	0,78	n.d.	n.d.	0,08	5,67	3,03	0,29	0,74	0,77	20,78	4,65	1,72	1,24	1,35	17,76	9,60	1,01	2,25	1,16	20,02	8,78
Mt. Rungwe (2016)	November	25	923	4,06	0,45	0,04	0,31	n.d.	5,90	1,78	0,03	0,84	0,70	18,29	3,11	1,11	0,87	0,13	13,74	5,80	0,51	0,80	0,12	41,43	6,95
		26	1723	8,25	0,49	0,04	0,48	0,09	9,77	2,97	0,42	0,64	1,13	22,55	5,10	2,66	0,77	1,12	16,20	8,55	1,28	1,04	1,01	30,87	2,63
		27	2580	15,63	0,42	n.d.	n.d.	0,17	8,04	2,36	0,40	0,93	1,58	24,00	3,84	2,67	0,55	1,19	14,93	6,70	1,30	0,80	1,24	13,25	8,75
		28	2797	12,10	0,68	n.d.	0,24	0,28	9,65	2,71	1,16	0,47	1,24	19,99	4,32	2,74	0,48	0,45	15,15	8,45	1,59	1,05	1,04	16,48	11,31
		29	400	0,95	0,14	n.d.	n.d.	0,29	3,55	2,79	0,78	2,21	1,11	20,21	6,54	2,63	1,26	4,24	20,32	8,97	2,23	2,81	5,56	13,40	2,69
		30	800	6,30	0,56	n.d.	n.d.	0,22	4,99	1,88	0,39	1,71	1,45	18,14	3,19	1,81	2,54	2,91	18,95	7,83	1,89	2,58	3,42	19,23	2,09
		31	1000	4,03	0,81	n.d.	n.d.	0,36	8,83	4,30	0,90	0,59	1,83	19,08	6,71	3,31	0,92	2,35	16,07	14,52	3,17	1,29	1,12	9,84	19,01
		32	1200	4,48	0,77	n.d.	n.d.	0,32	6,91	4,18	0,67	0,69	1,67	19,25	8,01	3,26	1,44	2,59	16,40	13,74	3,14	1,71	1,19	9,57	17,60
		33	1400	2,23	0,39	n.d.	n.d.	0,17	9,81	2,96	0,72	0,40	1,96	20,86	5,75	3,02	0,84	2,79	16,34	16,77	4,40	1,23	0,79	8,58	14,25
Mt. Majella (2016)	December	34	1600	4,94	0,85	n.d.	n.d.	0,39	10,83	4,23	1,41	0,64	1,43	21,11	6,70	2,74	0,57	1,68	14,93	15,44	2,71	1,00	1,00	7,41	8,65
		35	1800	2,99	n.d.	n.d.	n.d.	n.d.	5,70	4,00	1,75	n.d.	1,62	24,03	9,71	3,03	0,88	2,79	16,74	9,56	2,40	3,10	6,12	5,57	0,98
		36	2000	n.d.	n.d.	n.d.	n.d.	n.d.	4,95	3,51	0,63	1,32	1,62	25,01	8,25	3,04	1,18	1,99	18,92	9,96	2,81	2,27	5,12	9,41	0,78
		37	2400	2,53	0,68	n.d.	n.d.	0,29	6,10	4,19	0,89	0,84	1,63	20,85	8,95	3,33	1,12	2,75	17,07	13,33	3,06	1,65	1,37	9,37	12,05
		38	2600	2,47	0,55	n.d.	n.d.	0,18	8,75	3,55	0,80	0,68	1,69	19,38	4,33	4,11	0,64	3,05	18,92	12,16	3,18	1,27	1,09	13,20	14,91
		39	2800	3,62	0,59	n.d.	n.d.	0,14	10,80	3,42	0,87	1,05	1,82	19,14	4,38	3,38	0,62	3,35	14,86	16,04	3,77	0,79	3,12	8,23	21,28

Supplementary Table 3. Indices derived from brGDGTs for soils from Mt. Majella and MAAT estima

Altitude	MBT	MBT'5Me	CBT	MAAT estimate (°C)
400	0,21	0,62	0,27	10,9
800	0,15	0,56	0,54	9,0
1000	0,18	0,62	0,30	10,9
1200	0,16	0,55	0,30	8,8
1400	0,17	0,58	0,34	9,7
1600	0,20	0,48	0,61	6,6
1800	0,16	0,56	0,74	8,9
2000	0,17	0,54	0,34	8,5
2400	0,15	0,47	0,70	6,2
2600	0,20	0,47	0,21	6,2
2800	0,14	0,42	0,22	4,5

tes calculated using the global soil calibration by De Jonge et al. (2014).